Universidad de Oviedo

Facultad de Ciencias

Departamento de Física

MASTER THESIS

Simulaciones en Nano-Óptica

Numerical simulations in Nano-Optics

Rafael Méndez Camino

July 26, 2020

Supervised by:

Dr. Pablo Alonso González

Agradecimientos

Después de 5 años en la facultad, me gustaría agradecerle a Pablo Alonso González su supervisión en este trabajo, así como a Gonzalo Álvarez Pérez la ayuda que me ha brindado para lograr terminar este TFM. Y por supuesto a José Ignacio Martín Carbajo por el esfuerzo que realizado para que el máster saliera adelante, ya que si no fuera por eso no podría haber realizado este trabajo. Y en general agradecerle el trabajo a la Universidad de Oviedo y los profesores que he tenido estos años que me han hecho llegar aquí. Y cómo no, finalizar dándole las gracias a mis padres, familia y amigos que siempre están cuando se les necesita.

Abstract

Surface polaritons (hybrid light-matter waves occurring in metal-like materials) allow the study of light at the nanoscale. This is because, as a difference to what happens with light in conventional optics, surface polaritons allow for beating the diffraction limit, opening the door for controlling light at the nanoscale. In this work, we will study from numerical simulations how surface polaritons propagate within different environments, including strongly anisotropic media. Particularly, we will study how surface polaritons reflect at boundaries with isotropic, uniaxial, and biaxial media, and analyze how different parameters, both from a physical and a more purely numerical point of view, affect the results obtained. However, the simulations will be performed with light (the excitation is straightforward in this case), being able to extrapolate all the results obtained directly to SPs. This study will allow us to explore a range of different exotic optical phenomena, such as anomalous reflections and back-reflections. Finally, as anisotropic back-reflection observations have yet not been achieved, we propose an experimental scenario based on our simulations that might allow its visualization. All this work was carried out using the commercial software COMSOL MULTIPHYSICS.

Contents

List of Figures

Chapter 1

Introduction

1.1 Motivation

Nowadays, nano-optics is a very important scientific field consisting on the study and control of light at the nanoscale. Understanding and controlling light is a main objective of modern physics, and it has achieved a great progress, however, light-matter interactions have been addressed by the "classical", rather traditional, way, meaning that most studies have been limited by the diffraction limit of light.
This limit states that two objects separated by a distance d, smaller than λ/NA, being λ the wavelength of the incident light and NA the numerical aperture of the imaging lens, cannot be optically resolved due to diffraction:

$$d = \frac{\lambda}{2n\sin(\theta)} = \frac{\lambda}{2NA} \tag{1.1}$$

The diffraction limit constitutes an important disadvantage from a fundamental and technological point of view as the promising ideas of the nanotechnology and nanoscience fields cannot be applied. But it exists a physical concept with great potential to overcome this limitation, which is the excitation of surface waves called surface plasmon polaritons and surface phonon polaritons, known by its initials as SPPs and SPhPs, respectively. They consist of surface waves, originated by the coupling of photons with mobile or bound charges in metals or polar materials, that have the property to enhance and confine optical fields into deeply sub-diffracting volumes. Since years, this capability has boosted many different applications, allowing for controlling the emission and absorption of light, and also to mold its flux on the nanometer scale [1].
Thanks to these recent technological advances and the capability to control surface polaritons properties, there is a renewed interest in their use on different applications, such as for example, magneto-optic data storage, microscopy, solar cells, or biological sensors for

molecule detection. One of the most interesting aspects of SPPs for researchers in optics is the way they allow to concentrate and channel light using sub-wavelength structures, which could lead to miniaturized photonic circuits with length scales much smaller than those currently achieved [2].
In the last years, with the emergence of 2D layered materials, there has been important observations of a set of unique polaritonic excitations. For example, in graphene, a material that shows extraordinary properties in many different aspects, electrically tunable and highly confined SPPs were predicted and observed, opening the door to more efficient optoelectronics, bio-sensing and, generally, mid-infrared applications [3]. PhPs have also been observed in hexagonal boron nitride (h-BN), in which, for specific frequencies, PhPs exhibit hyperbolic behaviour and low losses, featuring ray-like propagation with high quality factors and hyper-lensing effects [4,5]. Also, in-plane anisotropic PhPs with extraordinary low losses have been also observed in the van der Waals biaxial crystal, α–MoO_3 [6].
Although the field of 2D material polaritonics and their hybrids is still emerging, it is already quite remarkable their potential for manipulating light–matter interactions across the visible, infrared and terahertz spectral ranges, allowing to control light one step further than the conventional studies.

In this final master thesis, it will be firstly shown some aspects about the basics about light-matter interactions and the general theory of polaritons at an interface between a semi-infinite anisotropic and a semi-infinite isotropic medium. After, it will be introduced the commercial software (COMSOL) allowing for carrying out full electromagnetic calculations of polaritons propagating at the nanoscale, thus allowing us to confront the analytical theory previously commented.
Finally, a study about reflections in the nanoscale will be carried out, taking into account the importance of the simulation software, including the need to have a clean simulation, a good mesh, etc. It will allow us to compare between reflections on different materials. To simplify the simulations, we will consider light instead of SPs, but all of the results obtained can be directly extrapolated to SPs, obtaining very interesting results and demonstrating why nanooptics is a very interesting field nowadays.

1.2 Basics about light-matter interactions

1.2.1 Overview

When someone wants to explain whatever about light, it is necessary to introduce the Maxwell's Equations [7]. As every physicist knows, these equations were summarized by

Maxwell in 1873 from all the previous knowledge about electricity and magnetism. They can lead us to obtain all the different connections between the fundamental parameters of electromagnetism: electric field ($\vec{E}$), magnetic field ($\vec{B}$, $\vec{H}$), the electric displacement field ($\vec{D}$), the electric current density ($\vec{J}$) and the electric charge density (ρ). As Maxwell did, we show in Equation (1.2.1) the relationship between these quantities in gaussian units and in their differential form.

$$\begin{aligned} \nabla \cdot \vec{D} &= 4\pi\rho, & \nabla \times \vec{E} + \frac{1}{c}\frac{\partial \vec{B}}{\partial t} &= 0, \\ \nabla \cdot \vec{B} &= 0, & \nabla \times \vec{H} - \frac{1}{c}\frac{\partial \vec{D}}{\partial t} &= \frac{4\pi}{c}\vec{J}, \end{aligned} \tag{1.2}$$

In addition to these equations, it is necessary to include some relations that explain the behavior of matter when it is acting an external field, known as material or constitutive relations. These equations are usually tricky, but in a simply way, when the field is time-harmonic (the time dependence is given by $exp(-i\omega t)$), the bodies are moving very slowly with respect to each other or in rest, and the material is isotropic, it is possible to express the constitutive relations as:

$$\vec{J} = \sigma\vec{E}, \qquad \vec{D} = \epsilon\vec{E}, \qquad \vec{B} = \mu\vec{H} \tag{1.3}$$

where σ represents the specific conductivity, ϵ represents the dielectric constant, also called permittivity, and μ represents the magnetic permeability. From these 3 parameters, we are more interested on ϵ, e. g. we are going to work with non-magnetic materials, so it is possible to take $\mu = 1$. The importance of ϵ lies in its direct dependence on the optical responses of materials, representing the capacity of the material to resist an electric field. The response of the material to an electric field depends on the frequency (ω) of itself, so the permittivity is a function of ω and is expressed as the complex function shown below:

$$\epsilon(\omega) = \epsilon'(\omega) + i\epsilon''(\omega) \tag{1.4}$$

As expected, ϵ' corresponds to the real part and ϵ'' is the imaginary of the permittivity, and the values taken classify the materials according to the following considerations:

- The real part of the permittivity accounts for the energy stored in the medium. In the simplest and most typical way, for a photon with a frequency given by ω, if $\epsilon(\omega)' < 0$, the light is screened, and the material behaves as a metal. In contrast, when the real part of permittivity is positive, the light can penetrate through the material, and the material behaves as a dielectric. Nevertheless, for specific frequencies in the infrared

spectral range (Restrahlen bands), it is possible to have a typical dielectric in the visible to behave like a metal with $\epsilon'(\omega) < 0$.

- The complex part is related to losses (energy losses). In a perfect dielectric, there are no free charges, so $\epsilon''(\omega)$ is 0 or near to zero (most of times, dielectrics are lossless materials). However, metallic materials have a lot of free charges, meaning a high conductivity, and the complex permittivity is given by $\epsilon''(\omega) = \frac{\sigma(\omega)}{\omega}$.

1.2.2 Electromagnetic waves

For isotropic linear dielectric media, from Maxwell's equations and assuming $\rho = 0$ and $J = 0$, it is possible to obtain the wave equations (1.5) and (1.6).

$$\nabla^2 \vec{E} - \frac{1}{v^2} \frac{\partial^2 \vec{E}}{\partial t^2} = 0 \tag{1.5}$$

$$\nabla^2 \vec{H} - \frac{1}{v^2} \frac{\partial^2 \vec{H}}{\partial t^2} = 0 \tag{1.6}$$

Where v is the speed of the light in a specific medium (Eq. (1.7)):

$$v = \frac{1}{(\epsilon\mu)^{1/2}} = \frac{1}{[(\epsilon_0\mu_0)(\epsilon_r\mu_r)]^{1/2}} = \frac{c}{(\epsilon_r\mu_r)^{1/2}} = \frac{c}{n} \tag{1.7}$$

Being ϵ_r and μ_r the relative permittivity and the relative permeability, respectively (as we have said, for non-magnetic materials $\mu_r = 1$), $c = (\epsilon_0\mu_0)^{-1/2}$ is the light speed in vacuum and $n = (\epsilon_r\mu_r)^{1/2}$ is the refractive index. In our case, the refraction index is:

$$n = \sqrt{\epsilon_r\mu_r} \overset{\mu_r=1}{=} \sqrt{\epsilon_r} \tag{1.8}$$

From Eq. 1.7, it is possible to consider harmonic fields of the form:

$$\vec{E} = \vec{E_0} e^{i\omega t} \quad \text{and} \quad \vec{H} = \vec{H_0} e^{i\omega t} \tag{1.9}$$

And if we take into account Equation (1.9), and $\omega = 2\pi\nu$, with ν the frequency, Equations (1.5) and (1.6) become into Equations (1.10) and (1.11):

$$\nabla^2 \vec{E_0} - \frac{\omega^2}{v^2} \vec{E_0} = 0 \tag{1.10}$$

$$\nabla^2 \vec{H_0} - \frac{\omega^2}{v^2} \vec{H_0} = 0 \tag{1.11}$$

The last 2 equations are known as Helmholtz equations.
Considering the solution in form of plane waves (Eq. (1.12) and (1.13)):

$$\vec{E} = Ae^{i(\omega t - \vec{k}\vec{r})} \tag{1.12}$$

$$\vec{H} = A'e^{i(\omega t - \vec{k}\vec{r})} \tag{1.13}$$

They represent a plane wave moving in the direction of positive r, that is a forward wave.
The vector $\vec{k}$ is the wave-vector, also known as wave number or propagation vector, and it is directed in the direction of the motion of the wave. Its modulus is $|\vec{k}| = k = 2\pi/\lambda$, where λ is the wavelength (in the medium).
From Equations (1.5) and (1.6) it is possible to determine that:

$$\frac{\omega^2}{k_0^2} = c^2 \quad \text{so} \quad k_0 = \omega/c = 2\pi/\lambda_0 \tag{1.14}$$

with λ_0 the wavelength in vacuum. When the wave is in a medium of refractive index n:

$$k = \frac{2\pi}{\lambda} = \frac{2\pi n}{\lambda_0} \tag{1.15}$$

Going a little further, it is possible to determine the direction in which energy propagates. This is given by the Poynting vector $\vec{S}$:

$$\vec{S} = \frac{1}{2}(\vec{E} \times \vec{H}) \tag{1.16}$$

It is important to note that for plane waves propagating in an isotropic medium the Poynting vector has the same direction of $\vec{k}$.

1.2.3 Absorption

Initially, the classical theory of absorption and dispersion of radiation was developed by Drude and Voigt, and finally fulfilled by Lorentz [8].
We know that the velocity of a wave in a specific material depends directly on the refraction index of this medium. Previously, we have said that the permittivity depends on frequency, $\epsilon(\omega)$, and n depends on ϵ_r, so n varies with the frequency, and can be also expressed as function of λ. This phenomenon is called dispersion, and a medium with this property is called dispersive medium.
For the classical Lorentz model for dielectrics, it is considered that the atom is formed by some oscillators with frequencies equal to the atomic absorption frequencies, ω_i. This oscillators are modelled as particles with mass m and charge e, and, under the action of

an oscillating electric field E, it is possible to write for the position vector $\vec{r}$ of the generic oscillator with proper frequency (eigenfrequency) w_0:

$$\ddot{\vec{r}} + \gamma\dot{\vec{r}} + \omega_0^2\vec{r} = -\frac{e}{m}\vec{E}e^{i\omega t} \tag{1.17}$$

with γ the damping factor. A solution for Equation (1.17) is:

$$\vec{r} = -\frac{(e/m)\vec{E}e^{i\omega t}}{(\omega_0^2 - \omega^2) + i\omega\gamma} \tag{1.18}$$

The oscillator has an electric dipole moment $\vec{P}$:

$$\vec{P} = -e\vec{r} \tag{1.19}$$

The polarization produced by the vibrating electric field $\vec{P}$, and assuming that all oscillators are equal and homogeneously distributed can be written as:

$$\vec{P} = -eN\vec{r} = N\alpha\vec{E}e^{i\omega t} = \epsilon_0\chi\vec{E}e^{i\omega t} \tag{1.20}$$

where χ is the susceptibility, N is the number of atoms (oscillators) per unit volume, and $\alpha = \epsilon_0\chi/N$ the polarizability, which is a complex number (Drude's formula), and can be written, thanks to Eq. (1.18) and (1.20), as:

$$\alpha = \frac{(e^2/m)}{(\omega_0^2 - \omega^2) + i\omega\gamma} \tag{1.21}$$

From Eq. (1.18), if ω is not near to ω_0, it is possible to neglect the imaginary term. Now, let us introduce a complex refractive index ($\hat{n}$):

$$\epsilon_r = \epsilon_r' + i\epsilon_r'' = 1 + \left(\frac{P}{\epsilon_0 E}\right) = (\hat{n})^2 = (n - ih)^2 \tag{1.22}$$

where ϵ_r is the complex relative permittivity, n is the real part of $\hat{n}$ and h its imaginary part. So we have:

$$(\hat{n})^2 = (n^2 - h^2) - i(2nh) = 1 + N\alpha/\epsilon_0 =$$

Using Eq. (1.21):

$$\begin{aligned} &= 1 + (N/\epsilon_0)[Re(\alpha) + Im(\alpha)] = \\ &= 1 + \left(\frac{e^2N}{\epsilon_0 m}\right)\left(\frac{\omega_0^2 - \omega^2}{(\omega_0^2 - \omega^2)^2 + \omega^2\gamma^2}\right) - i\left(\frac{e^2N}{\epsilon_0 m}\right)\left(\frac{\gamma\omega}{\omega_0^2 - \omega^2)^2 + \omega^2\gamma^2}\right) \end{aligned} \tag{1.23}$$

In a low density gas it is possible to approximate: $k << 1$, $|n-1| << 1$ and $n^2-1 = 2(n-1)$, leading to:

$$n = 1 + \left(\frac{e^2 N}{\epsilon_0 m}\right)\left(\frac{\omega_0^2 - \omega^2}{(\omega_0^2 - \omega^2)^2 + \omega^2\gamma^2}\right) \tag{1.24}$$

And then:

$$h = \left(\frac{e^2 N}{\epsilon_0 m}\right)\left(\frac{\gamma\omega}{(\omega_0^2 - \omega^2)^2 + \omega^2\gamma^2}\right) \tag{1.25}$$

If we make $k = \hat{n}k_0 = (n - ih)k_0$, we obtain:

$$E = A \cdot \exp\left(i[\omega t - (n - ih)k_0 x]\right) = A \cdot \exp\left[-(hk_0 x)\right] \exp\left[i(\omega t - nk_0 x)\right] \tag{1.26}$$

that represents a wave with wave vector nk_0, propagating along the x-axis, with its amplitude decaying exponentially as the wave travels within the medium. This behaviour is known as Beer's law. It is possible to define the intensity in terms of the absorption coefficient β:

$$I = I_0 e^{-\beta x} \tag{1.27}$$

where $\beta = 2k_0 h$. h is part of the refraction index, such as increasing the absorption in a material it also increases.

1.2.4 Drude-Lorentz model for metals

To explain the optical response of polar and metallic materials, it exits different models, being the simplest the Drude or Drude-Loretnz [8]. In the Drude-Lorentz model, electrons are free, and from the previous equations $\omega_0 = 0$, which means that there is no restoring force. In this model, the metal consist of a free electron gas with a free electron density, N, and it moves against a fixed lattice background of positive ion cores.
Importantly, in the Drude-Lorentz model, the lattice potential and electron-electron interactions are not taken into account. However, some details and aspects of the band structure are include into the effective optical mass of each electron, m. This plasma model is known as the Drude model.
If we repeat some calculations from the previous point but with this model, one can obtain the Equation (1.28), for the dielectric constant (complex).

$$\epsilon(\omega) = 1 - \frac{\omega_p^2}{\omega^2 - i\gamma\omega} \tag{1.28}$$

In this equation, γ corresponds to the damping factor and ω_p is the plasma frequency of the metal, represented in Equation (1.29), which depends on the free electron density (N) of the

metal.

$$\omega_p = \sqrt{\frac{Ne^2}{\epsilon_0 m}} \tag{1.29}$$

Here e is the electron charge, m the electron mass and ϵ_0 the permittivity of the vacuum. From this, it is possible to determine the real ($\epsilon'(\omega)$) and imaginary ($\epsilon''(\omega)$) parts of the permittivity:

$$\epsilon'(\omega) = 1 - \frac{\omega_p^2 \tau^2}{1 + \omega^2 \tau^2} \tag{1.30}$$

$$\epsilon''(\omega) = \frac{\omega_p^2 \tau^2}{\omega(1 + \omega^2 \tau^2)} \tag{1.31}$$

where $\tau = \gamma^{-1}$ is the relaxation time of electrons taking values of about 10^{-14}s. In the case of a gas of free electrons, the relaxation time, τ is the characteristic time for a electrons distribution to reach the equilibrium once there is no disturbances and γ is a phenomenological damping constant.
In optics, the usual working frequency range is below the ultraviolet. If $\omega < \omega_p$, and $\omega\tau >> 1$, the permittivity is real, and it can be written as:

$$\epsilon(\omega) = 1 - \frac{\omega_p^2}{\omega^2} \tag{1.32}$$

In the other hand, at low frequencies, $\omega << \tau^{-1}$, which means $\epsilon'' >> \epsilon'$. With respect to the refractive index, both real part and imaginary part are of comparable magnitude:

$$n = h = (\epsilon''/2)^{1/2} = \left(\frac{\tau\omega_p^2}{2\omega}\right)^{1/2} \tag{1.33}$$

In this frequency region metals have a great absorption, the absorption coefficient, β, is defined as:

$$\beta = \left(\frac{2\omega\tau\omega_p^2}{c^2}\right)^{1/2} \tag{1.34}$$

The fields decays inside the metal as a result of $e^{-x/\delta}$, where δ is the skin depth:

$$\delta = \frac{2}{\beta} = \frac{c}{h\omega} \tag{1.35}$$

When photon energies are below the threshold of transition between electronic bands, for metals, the optical response is well described by the dielectric function of the Drude model. If a more practical treatment is needed, it is possible to integrate the Drude model using Eq. (1.17), and describing each transition between bands in a classical way of a bound electron with resonance frequency ω_j. Each band transition leads to a Lorentz-oscillator term of the

form $A_i/(\omega_i^2 - \omega^2 - i\gamma\omega)$ that have to be added to the free electron result, so:

$$\epsilon(\omega) = \epsilon_\infty - \sum_{j=1}^{q} \frac{f_j \omega_p^2}{[(\omega_j^2 - \omega) + i\gamma_j \omega]} \tag{1.36}$$

Being ϵ_∞ a suitable constant, q is the number of oscillators with frequency ω_j, f_j is the strength and $1/\gamma_j$ is the lifetime.
For metals, the absorption is related with the conductivity σ. The current density is defined as:

$$j = -Nev \tag{1.37}$$

Where v is the drift velocity of electrons, if we substitute it into Eq. (1.17), and with $\omega_0 = 0$:

$$\frac{dj}{dt} + \gamma j = \left(\frac{Ne^2}{m}\right) E \tag{1.38}$$

We can use a local approximation to the current-field relation, assuming that the temporal dependence of E and j are:

$$E = E_0 e^{-i\omega t} \tag{1.39}$$

And

$$j = j_0 e^{-i\omega t} \tag{1.40}$$

Replacing it in (1.38):

$$j = \left(\frac{Ne^2\tau}{m}\right)\left(\frac{1}{1 - i\omega\tau}\right) E = \sigma E \tag{1.41}$$

In the case of a static field, where $\omega = 0$, it is defined the static conductivity:

$$\sigma_{st} = \frac{Ne^2\tau}{m} \tag{1.42}$$

Now, for the most general case, in which it is applied an oscillating field, the conductivity becomes complex and dynamic:

$$\sigma = \frac{Ne^2\tau}{m} \frac{1}{1 - i\omega\tau} \tag{1.43}$$

For some particular conditions it is possible to obtain a purely real or purely imaginary conductivity, e. g., for very low frequencies, which means $\omega\tau << 1$, the conductivity is purely real and electrons and electric field oscillate with the same phase. If we start increasing the frequency of the applied field, the electrons acquire inertia, that induces a phase lag, and the conductivity becomes complex. In the case of using optical frequencies and above, that is $\omega\tau >> 1$, the dynamic conductivity is purely imaginary and the electrons oscillate 90° out of phase with respect to the incident electric field. The Drude conductivity is proportional

to the relaxation time of the material. It is possible to express the conductivity in a complex form:

$$\sigma = \sigma' + i\sigma'' \tag{1.44}$$

with:

$$\sigma' = \left(\frac{Ne^2\tau}{m}\right)\left(\frac{1}{1+\omega^2\tau^2}\right) \tag{1.45}$$

and

$$\sigma'' = \left(\frac{Ne^2\tau}{m}\right)\left(\frac{\omega\tau}{1+\omega^2\tau^2}\right) \tag{1.46}$$

Relating this expression with Eq. (1.30) and (1.31), we obtain:

$$\epsilon' = 1 - \frac{\sigma'}{\epsilon_0\tau} \tag{1.47}$$

and

$$\epsilon'' = \frac{\sigma''}{\epsilon\tau\omega} \tag{1.48}$$

Similar considerations can be done for dielectric materials, and also semiconductors, which present spectral regions with a negative permittivity. Two dimensional plasmonic materials (such as graphene) can be treated using this model, as well as topological insulators, which are materials that behave as an insulator in its interior but at the surface there are conducting states.

Other interesting material examples that can be fitted with this simple model are h-BN or MoO_3, which show a very interesting hyperbolic propagation of light, as we will see in next sections.

1.2.5 Pulses and group velocity

A wave packet with a frequency distribution is a pulse (with finite duration). We can describe its propagation in a linear medium as a superposition of plane waves of different frequency:

$$\Psi(x,t) = \int A(k)e^{i(\omega t - kx)}dk \tag{1.49}$$

where $A(k)$ gives the amplitude of the plane wave, and k is the wavevector. At $t = 0$, $A(k)$ is the Fourier transform of $\Psi(x,0)$ and $|A(k)|^2$ is the Fourier spectrum of $\Psi(x,t)$. The relationship between ω and k is the dispersion relation, but in an isotropic medium, the dispersion properties do not depend on the direction of propagation, so:

$$\omega(k) = \omega(-k)$$

The parameters that characterize a pulse are its central frequency ω_0, and the frequency width $\Delta\omega$, around the central frequency, which means that $A(k)$ is sharply peaked around k_0. If we want to study the time evolotion of a pulse, we have to expand the frequency as a Taylor series around k_0:

$$\omega(k) = \omega_0 + \left(\frac{d\omega}{dk}\right)_0 (k - k_0) + \frac{1}{2}\left(\frac{d^2\omega}{dk^2}\right)_0 (k - k_0)^2 + ... \tag{1.50}$$

From Eq. (1.49), considering only the first term of the expansion, we have:

$$\Psi(x,t) = \exp\left(i[\omega_0 t - kx]\right) \int A(k) \exp\left(i[\left(\frac{d\omega}{dk}\right)_0 t - x][k - k_0]\right) dk \tag{1.51}$$

This integral corresponds to a Fourier transform of a function of the type:

$$E[x - \left(\frac{d\omega}{dk}\right)_0 t]$$

So, it is possible to write the amplitude of the pulse as:

$$\Psi(x,t) = \exp\left(i[\omega_0 t - kx]\right) E[x - \left(\frac{d\omega}{dk}\right)_0 t] \tag{1.52}$$

From Eq. (1.52) we can determine the group velocity. This equation represents a signal carried by a frequency ω_0 and modulated by a curve $E[x - \left(\frac{d\omega}{dk}\right)_0 t]$. And this modulation curve moves with a velocity:

$$v_g = \frac{dx}{dt} = \frac{d\omega}{dk} \tag{1.53}$$

which is the group velocity. When, in a given medium, the phase velocity is constant and does not depend on the frequency, it means that $v_g = v_p$. This approximation is correct only if the distribution $A(k)$ is sharply peaked at k_0 and the frequency is a smoothly varying function of k around k_0. Also, if the electromagnetic energy density of the pulse is related with the square of the amplitude, v_g represents the transport of energy.
In a medium with refractive index n, the phase velocity is given by:

$$v_p = \frac{c}{n(\omega)} \tag{1.54}$$

which can be larger or smaller than the speed of light, depending if n is larger or not than the unit. The relationship between k and ω is:

$$k = n(\omega)\frac{\omega}{c} \tag{1.55}$$

Calculating the group velocity from Eq. (1.53), we obtain:

$$v_g = \frac{c}{n_g} = \frac{c}{n + \omega(dn/d\omega)} \tag{1.56}$$

being n_g the group index:

$$n_g = n + \omega \left(\frac{dn}{d\omega} \right) \tag{1.57}$$

1.3 Optically anisotropic media

Hitherto, we have only taken into account isotropic materials, that is, materials with the same response to electromagnetic fields in all direction of space. This type of materials are always used for pedagogical examples, as it is easier to calculate their response; however, more exotic and thus interesting optical phenomena can be observed in anisotropic materials (and thus our interest on them in this work).
As we have shown in Eq. (1.3), we can relate $\vec{D}$ with $\vec{E}$ by the permittivity, which in the most general case is a tensor of the form:

$$\hat{\epsilon} = \begin{pmatrix} \epsilon_{xx} & \epsilon_{xy} & \epsilon_{xz} \\ \epsilon_{yx} & \epsilon_{yy} & \epsilon_{yz} \\ \epsilon_{zx} & \epsilon_{zy} & \epsilon_{zz} \end{pmatrix}$$

This is because anisotropic materials usually have different values of ϵ in each direction. Taking the appropriate coordinate system, it is always possible to make this tensor diagonal such as:

$$\hat{\epsilon} = \begin{pmatrix} \epsilon_x & 0 & 0 \\ 0 & \epsilon_y & 0 \\ 0 & 0 & \epsilon_z \end{pmatrix}$$

The components of the tensor, ϵ_x, ϵ_y and ϵ_z are the complex permittivities of the material in the 3 directions (x, y and z respectively). The simplest case is thus the isotropic case, where $\epsilon_x = \epsilon_y = \epsilon_z = \epsilon$.
Note that using the correct system of axes (principal axes), it is possible to write Eq. (1.3) as:

$$\begin{pmatrix} D_x \\ D_y \\ D_z \end{pmatrix} = \begin{pmatrix} \epsilon_x & 0 & 0 \\ 0 & \epsilon_y & 0 \\ 0 & 0 & \epsilon_z \end{pmatrix} \begin{pmatrix} E_x \\ E_y \\ E_z \end{pmatrix} = \epsilon_0 \begin{pmatrix} n_x^2 & 0 & 0 \\ 0 & n_y^2 & 0 \\ 0 & 0 & n_z^2 \end{pmatrix} \begin{pmatrix} E_x \\ E_y \\ E_z \end{pmatrix}$$

1.3.1 Uniaxial and biaxial crystals

When the permittivity for one of principal axes of the tensor is different from the other and these are equal, the material is referred as uniaxial [9, 10]. The axis that is different is called the *optical axis*. If we assume that z-axis is the optical axis, and the other two are equal (*i. e.*, $\epsilon_x = \epsilon_y \neq \epsilon_z$), the permittivity tensor can be expressed as:

$$\hat{\epsilon} = \begin{pmatrix} \epsilon_\perp & 0 & 0 \\ 0 & \epsilon_\perp & 0 \\ 0 & 0 & \epsilon_\parallel \end{pmatrix}$$

Where $\epsilon_\parallel = \epsilon_z$ representing the parallel component to the optical axis, and $\epsilon_x = \epsilon_y = \epsilon_\perp$ represent those components perpendicular to it.

Furthermore, there is another possibility apart from isotropic or uniaxial materials, i.e. when the permittivity is different in all directions of space (that is a material characterized by three refractive indices). In this case, the material is known as biaxial. Although there is no axis of symmetry, there are 2 optical axes or binormals which are defined as directions along which light may propagate without birefringence. The 3 cases of materials classified according to its permittivity form are represented in Figure 1.1. Figure 1.1(a) represents an isotropic material, in which all refractive indexes (directly related with the permittivity) are equal in all directions, represented with a blue color. Figure 1.1(b) corresponds to an elliptic uniaxial material where the optical axis is the z-axis, and the other axes are optically equal. Finally, Figure 1.1(c) represents a biaxial material, where the 3 directions are optically different.

To study the propagation of light in a certain medium, we make use of the dispersion $\omega(\vec{k})$, where $\vec{k}$ is the wavevector, $\vec{k} = (k_x, k_y, k_z)$, and ω is the frequency. Particularly, the wavevector describes the number of oscillations that the wave completes per space unit, so it is related with the wavelength as $\lambda = 2\pi/|\vec{k}|$. Interestingly, a solution of the dispersion relation (generally a 3D complex function) for a given frequency leads to what is typically called an isofrequency curve. The isofrequency curve is useful to describe the propagation of light inside a certain medium in a graphical way, showing which directions (wavevectors) can propagate through a medium for a given frequency ω.

In the simplest case, when light propagates in vacuum, the isofrequency curve has the following form:

$$k_x^2 + k_y^2 + k_z^2 = \frac{\omega^2}{c^2} = k^2 \tag{1.58}$$

i.e. a sphere with radius ω/c. By simply plotting it we obtain a direct visualization of the direction of propagation of light, Figure 1.2(a). If, instead of vacuum, we have an isotropic medium, we also have a sphere but enlarged, due to the different norm of the permittivity

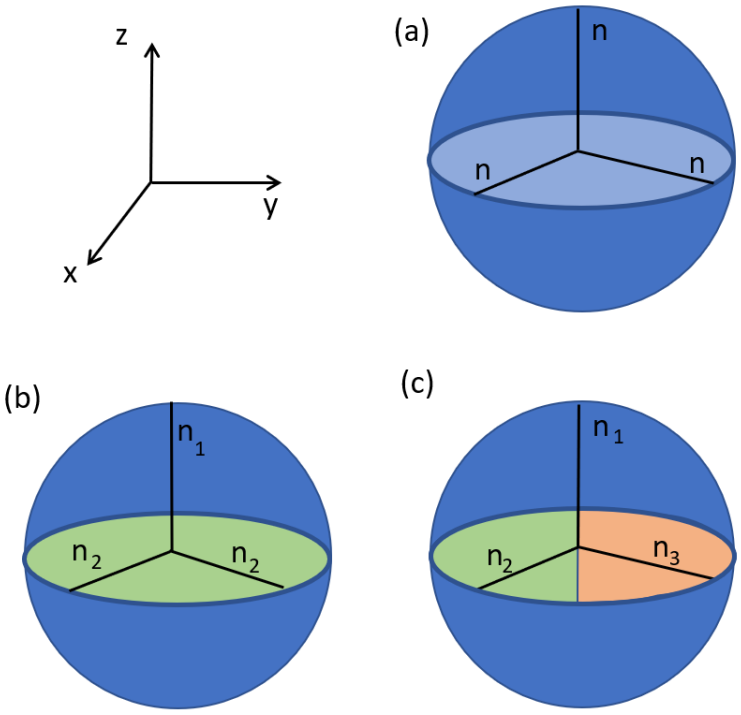

Figure 1.1: Representation of 3 different types of materials: **(a)** is a isotropic material, with the same permittivity in the 3 axis, **(b)** is a uniaxial material, with n_1 the refraction index of the optic axis, which corresponds to the z-axis (it also corresponds to $\epsilon_{\|}$), **(c)** represents a biaxial material, with 3 different permittivities.

(ϵ), which changes Equation (1.58) in $k^2 = \epsilon^2 \frac{\omega^2}{c^2}$.

When light propagates in a uniaxial material the equation changes a little, and the isofrequency curve is not anymore an sphere but an ellipsoid or a hyperbola, given by:

$$\frac{k_x^2 + k_y^2}{\epsilon_{\|}} + \frac{k_z^2}{\epsilon_{\perp}} = \frac{\omega^2}{c^2} \tag{1.59}$$

In case that $\mathrm{Re}(\epsilon_{\|}) > 0$ and $\mathrm{Re}(\epsilon_{\perp}) > 0$, the curve represents an ellipsoid, as shown in Figure 1.2(b). If the anisotropy of the crystal is such that one of the signs of the permittivity in one direction is opposite to the other two, the curve of the isofrequency is a hyperboloid and the material behaves as a metal for the direction where the permittivity is negative and as a dielectric in the other two directions.

Hyperbolic materials can also be biaxial, in this case the permittivity values with the same sign possess different norm. There are two main groups where hyperbolicity in uniaxial materials can be classified, which are known as *type-I* and *type-II*.

For type-I, the isofrequency surface is a two-sheeted hyperbola (Figure 1.2(c), Type I), corresponding to: $\mathrm{Re}(\epsilon_{\|}) < 0$ and $\mathrm{Re}(\epsilon_{\perp}) > 0$. However, type-II surface is a single-sheeted

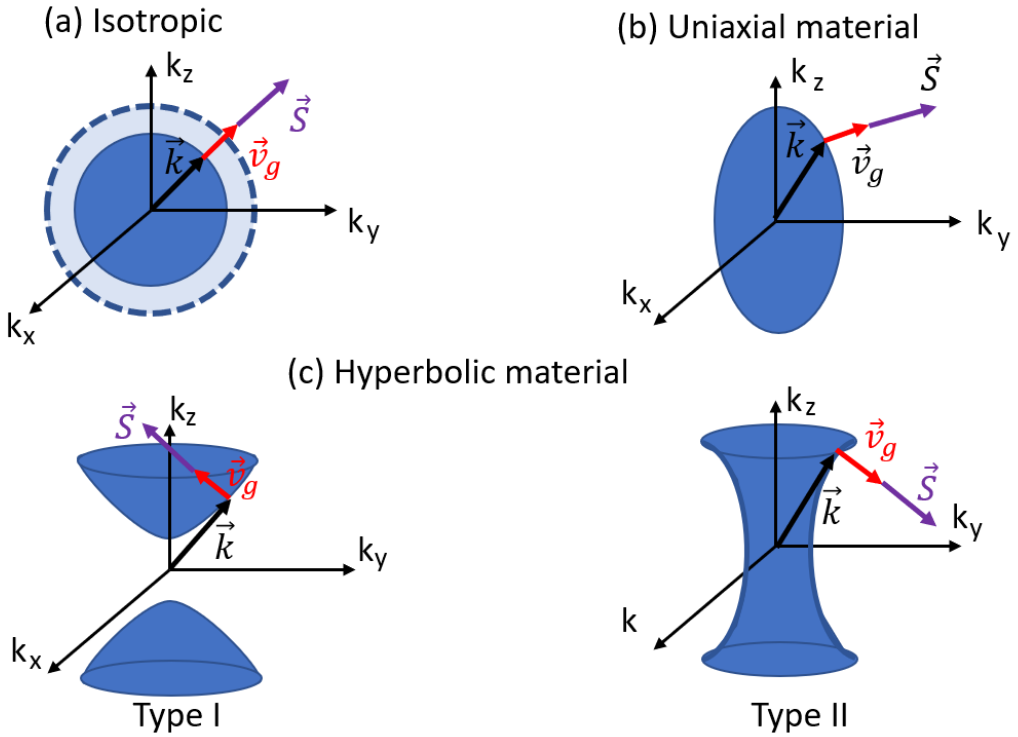

Figure 1.2: Isofrequency curves for different materials: **(a)** vacuum or isotropic dielectric (dashed lines), **(b)** positive uniaxial material, where $\epsilon_{\parallel} > \epsilon_{\perp} > 1$, it corresponds to an elliptic material, **(c)** hyperbolic with 2 possible cases, Type I means $\epsilon_{\parallel} < 0$ and $\epsilon_{\perp} > 0$, and Type II means $\epsilon_{\parallel} > 0$ and $\epsilon_{\perp} > 0$. Adapted from [11].

hyperbola (Figure 1.2(c), Type II), because two components of the permittivity tensor have negative signs, $\mathrm{Re}(\epsilon_{\parallel}) > 0$ and $\mathrm{Re}(\epsilon_{\perp}) < 0$.

Classifying hyperbolicity in biaxial materials is a little more complicated certainly going beyond the purpose of this master thesis.

It is important to highlight that the wavevector $\vec{k}$, related with the phase velocity ($v_p = \omega/k$), does not always represent the direction of propagation of light, in stark contrast to what we typically observe in isotropic media. Note that the direction of propagation of a wave is given by the group velocity, ($v_g = \partial\omega/\partial k$), which is also the direction where the energy flows, which is usually expressed by the Poynting vector ($\vec{S} = \vec{E} \times \vec{H}$). Looking again to Figure 1.2, for materials with strong anisotropy, $\vec{S}$ and $\vec{k}$ are not generally parallel, and in hyperbolic materials they can be almost perpendicular. Actually, for large $\vec{k}$ values, the Poynting vector is perpendicular to $\vec{k}$, and $\vec{S}$ (and also v_g) has a fixed angle with respect to the optical axis. This makes possible to have a material where v_p and v_g show an opposite sign for a specific direction, leading into very exceptional optical phenomena, such as negative refraction or the propagation of backward waves [6].

Another interesting phenomena occurs when light is reflected in anisotropic materials, an

particularly when considering coupled oscillations of photons and electrons, i.e. the quasi-particle called surface polariton.

1.4 Surface Polaritons

Now, that we have remembered the main characteristics of light-matter interactions and light propagation, it is time to go one step further. As our goal is simulate and study reflections in different materials, in which surface waves (surface polaritons, SP) emerge at the boundary between anisotropic media and air, we are going to explain what a SP is and the different types of SP that we can have.
In the most simply way, surface polaritons are waves that propagate along the surface of a material with negative permittivity, such as a metal in the visible spectral range or a polar dielectric in the infrared. They can be seen as light waves trapped on a surface due to the interaction with material excitations, such as collective oscillations of free electrons (plasmons) or lattice vibrations (phonons), which try to screen out the impinging field. Importantly, these surface waves exhibit unique properties as we will see in the following.

1.4.1 Surface Plasmon Polaritons (SPPs)

More accurately, SPPs are quasiparticles arising from the coupling of electromagnetic waves with an electric or magnetic dipole-carrying excitation in matter, such as excitons, phonons or plasmons (Fig. 1.3). Although Maxwell's equations are defined for continuous regions, SPPs can exist at interfaces, as we have said previously, and in the bulk, which will not be covered here.
The most common surface excitations are the surface plasmon polaritons (SPPs), which are excitations in the infrared or in the visible spectral range that propagate trough the interface between a conductor and a dielectric, being evanescently confined in the perpendicular direction to the surface. These waves are due to the coupling of the electromagnetic fields to collective oscillations of the conductor's electron plasma.

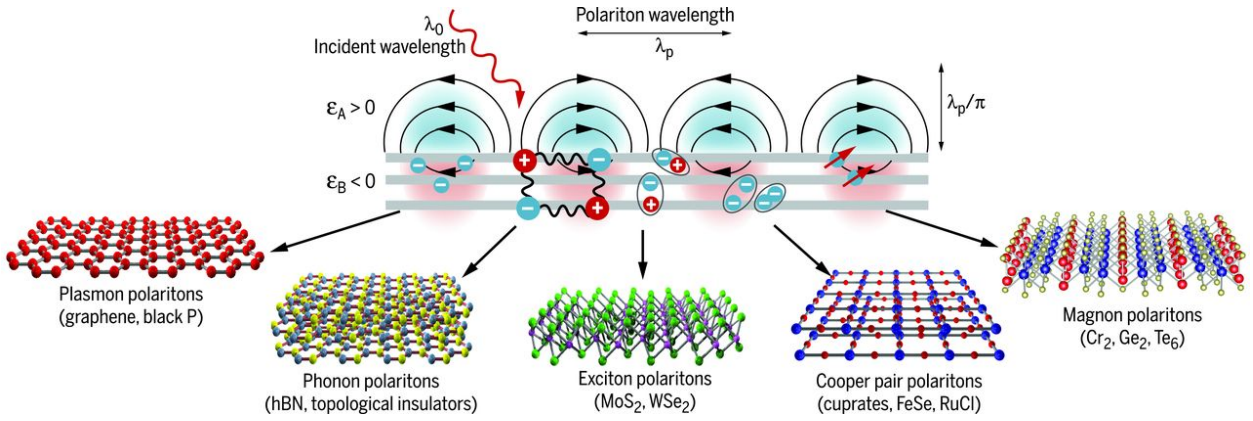

Figure 1.3: Polaritons, a hybrid of light-matter oscillations, can originate from different material excitations, such as conduction electrons in graphene and topological insulators (SPPs), infrared-active phonons in boron nitride (SPhPs), excitons in dichalcogenide materials (exciton polaritons), superfluidity in FeSe- and Cu-based superconductors with high critical temperature T_c (Cooper-pair polaritons), and magnetic resonances (magnon polaritons). The matter oscillation component results in negative permittivity ($\epsilon_B < 0$) of the polaritonic material, giving rise to optical-field confinement at the interface with a positive-permittivity ($\epsilon_A > 0$) environment. VdW polaritons exhibit strong confinement, as defined by the ratio of incident light wavelength λ_0 to polariton wavelength λ_P . From [12].

The interaction between the surface charges and the electromagnetic field that constitutes the SPP has two consequences [2]:

- On the one hand, the interaction between the electromagnetic field and the surface charge density results in the momentum of the SPP mode, which is $\hbar k_{SP}$ being greater than the momentum of a free-space photon of the same frequency, $\hbar k_0$ (where $k_0 = \omega/c$ is the free-space wavevector). Solving the Maxwell's equations with the appropriate boundary conditions, it shows the SPPs dispersion relation:

$$k_{SP} = k_0 \sqrt{\frac{\epsilon_d \epsilon_m}{\epsilon_d + \epsilon_m}} \tag{1.60}$$

  where ϵ_m is the permittivity of the metal, which depends on the frequency, and ϵ_d that of the dielectric. Both of them must have different signs if SPPs are to be possible at such an interface. This is possible in metals on air because the permittivity is negative in the former and positive in the latter. The increase in momentum is associated with the binding of the SPPs to the surface.

- On the other hand, the field perpendicular to the surface decays exponentially with distance from it, which prevents power from propagating away from the surface.

Once a SPP is excited on the surface of a metal, it will propagate but will gradually attenuate owing to losses arising from the absorption of the metal. The attenuation depends on the

dielectric function of the medium at a given frequency, that is the oscillation frequency of the SPP. The propagation length can be calculated from Equation (1.61).

$$\delta_{SP} = \frac{1}{2k''_{SP}} = \frac{c}{\omega}\left(\frac{\epsilon'_m + \epsilon_d}{\epsilon'_m \epsilon_d}\right)^{3/2} \frac{(\epsilon'_m)^2}{\epsilon''_m} \tag{1.61}$$

where k''_{SP} is the complex surface plasmon wavevector, $k_{SP} = k'_{SP} + ik''_{SP}$, from Eq. (1.60), and $\epsilon_m = \epsilon'_m + i\epsilon''_m$. As a fact silver is the metal with the lowest losses in the visible spectrum, with typically a propagation distances in the range 10–100 μm. Years ago, absorption by the metal was a significant problem for SPPs, that they were not considered viable for photonic elements. This view has changed thanks to the recent demonstrations of SPP-based components that are significantly smaller than the propagation length. These developments give the possibility to integrate many devices based on SPPs into circuits before propagation losses become too significant.
Furthermore, SPPs have other uses in other photonic technologies, for example, they excel in light generation. Thanks to their capability to enhance and confine light into subwavelength scales, SPPs are considered a basic building block in nanophotonics.

1.4.2 Surface Phonon Polaritons (SPhPs)

SPhPs are very similar to SPPs, while SPPs can concentrate light to subwavelength scales in conductors, SPhPs concentrate light to subwavelength scales in polar dielectrics. They are the result of coupling light to polar optical phonons (Fig. 1.4).
As an introduction, the main technological inconvenience of SPPs is the high optical losses inherent to metals at optical frequencies. Also, while plasmonics in metals has been successfully demonstrated in the UV to NIR spectral range, the very large negative permittivity at longer wavelengths limits its usefulness beyond the NIR. It is thus necessary to search into alternative low-loss optical materials supporting surface waves. One of the alternatives consist on exploring the use of dielectric materials.
Actually, dielectric materials give a very interesting opportunity to achieve sub-diffraction confinement, low optical losses and operation in the mid-IR to THz spectral ranges thanks to the excitation of SPhPs modes.
Particularly, it is possible to excite SPhPs in polar dielectrics materials between the longitudinal (LO) and transverse optic (TO) modes of the phonon frequencies, the spectral range that is known as the "*Reststrahlen*" band. In this case, the mechanisms governing optical losses come from the scattering of optical phonons, which usually occurs on time-scales in excess of a picosecond. That means an important reduction in the optical losses of the SPhPs modes in comparison with SPPs (e-e scattering occurs in the fs scale) [13].

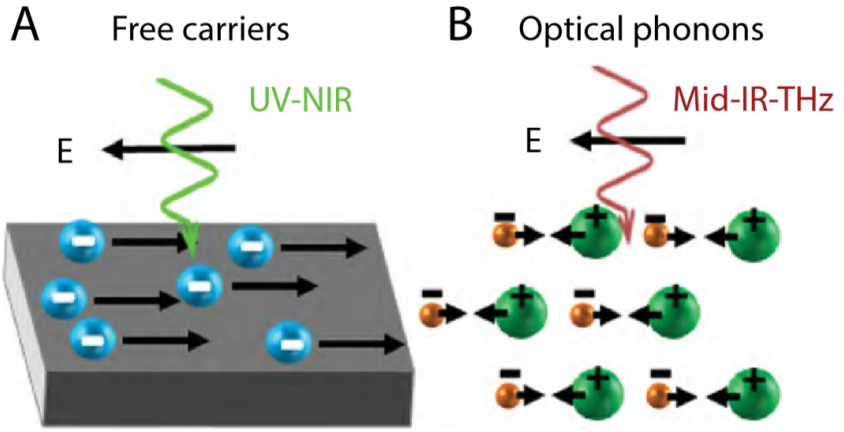

Figure 1.4: Schematic illustration of collective oscillations of (A) free carriers in metals and (B) atomic displacements in the form of optical phonons in polar dielectrics. From [13].

The interaction between optic phonons in polar materials and electromagnetic waves can be explained with Maxwell's equations, similarly than we have done before for SPPs. Considering an incident plane wave with $\vec{k}$ the wavevector, and no free charges in the medium ($\rho = 0$), and using the first equation from Eq. (1.2.1), with $\vec{D}$ the electric displacement vector:

$$\nabla \cdot \vec{D} = 0$$

which is equivalent to:

$$\epsilon(\omega)(\vec{k} \cdot \vec{E}) = 0 \tag{1.62}$$

Eq. (1.62) has 2 solutions:

- Solution 1: $\epsilon(\omega) = 0$. This solution corresponds to the longitudinal mode (LO), with a longitudinal resonance frequency $\omega = \omega_L$.
- Solution 2: $\vec{k} \cdot \vec{E} = 0$. This is the solution of the transversal mode (TO), which has a transversal resonance frequency $\omega = \omega_T$.

As said before, the spectral range of existence of SPhPs occurs between these 2 frequencies and is called Reststrahlen band. When a plane wave with frequency ω, in the Reststrahlen band, impinges on a polar dielectric surface, the positive charges associated to the lattice vibration move along the direction of the incident field, and the negative charges move against it. The result, as a consequence of the real part of the permittivity being negative in this spectral range, is that the polar dielectric behaves like a metal in the visible.
The most common crystals that supports SPhPs are SiC, GaAs or quartz, and some uses for SPhPs could be data storage, thermal emission or molecule sensing, etc [1].

1.5 Numerical simulations. COMSOL

1.5.1 About COMSOL

COMSOL (COMSOL Multiphysics Modelling Software) is a software that solves Maxwell's equations. The own COMSOL website describes their software as [14]:

"*COMSOL Multiphysics® is a general-purpose simulation software for modeling designs, devices, and processes in all fields of engineering, manufacturing, and scientific research. In addition to using multiphysics modeling for your own projects, you can also turn your models into simulation applications and digital twins for use by other design teams, manufacturing departments, test labs, customers, and more.*
The platform product can be used on its own or expanded with functionality from any combination of add-on modules for simulating electromagnetics, structural mechanics, acoustics, fluid flow, heat transfer, and chemical engineering. The add-on modules and LiveLink™ products connect seamlessly for a modeling workflow that remains the same regardless of what you are modeling."

COMSOL uses finite elements for analysis and is also a multiphysics simulation software. It allows conventional physics-based user interfaces and coupled systems of partial differential equations (PDEs). COMSOL provides an integrated development environment (IDE) and unified workflow for optical, electrical, mechanical, fluid, acoustics and chemical applications. In the next chapter we will explain the main features of COMSOL in more detail, explaining about the interface, how to use it, and, of course, the results that can be obtained showing our simulations on reflection.

1.5.2 Why COMSOL?

COMSOL is one of the most complete software available, in which you can study thermodynamic problems, how a system evolves in time, fluids, and, of course, the optical behaviour of a system. COMSOL allows the user to control all steps of the simulation process, you can define the geometry, the properties and the physics that your system/material has, being able to describe the phenomena that we want.
In spite of all different software that solve Maxwell equations numerically, we have chosen COMSOL because it offers for the user (us) all the steps in the modeling workflow. For example, as we will show in next chapter, we can define geometries with the properties and physics that we specifically want in our model, i. e., we can exactly define the system and phenomena that we have in our experiment.
Another important point for COMSOL is the capability to show how our systems evolves

in time, (in addition to, of course, study the optical behaviour simulating, e. g., Gaussian beams).

1.5.3 Gaussian Beams

COMSOL can work with gaussian beams, and we are going to use it in our work. Gaussian beams are a particular solution for Maxwell equations with axial symmetry [8]. The name of Gaussian beams comes from the shape of the transversal profile of the beam (obviously Gaussian shape). Let us consider a beam that propagates in the z direction, where the electric field at any position z is given in the (x, y) plane:

$$E = E_0 \left(\frac{w_0}{w}\right) \exp\left[-i(kz+\Psi) - (x^2+y^2)\left(\frac{ik}{2}\right)\left(\frac{1}{R} - \frac{2i}{kw^2}\right)\right] = \\ = E_0 \left(\frac{w_0}{w}\right) \exp\left[-\left(i[kz+\Psi] - ik\frac{(x^2+y^2)}{2R}\right)\right] \exp\left[-\frac{(x^2+y^2)}{w^2}\right] \tag{1.63}$$

Here, E is the electric field, and it has a maximum at $z = 0$. The parameter w_0 represents the minimum beam width also at $z = 0$, w is called beam waist and represent the beam width at a distance z:

$$w(z) = w_0 \left[1 + \left(\frac{z\lambda}{w_0^2 n\pi}\right)^2\right]^{1/2} \tag{1.64}$$

Looking at Eq. (1.64), we see that a Gaussian beam depends on the wavelength, but there are other parameters that also influence the beam. At $z = 0$, the Gaussian beam has the form of a plane wave, but it if z is increased, the beam changes to a curved wave front of radius R. The radius of curvature is:

$$R(z) = z\left[1 + \left(\frac{w_0^2 k}{2z}\right)^2\right] \tag{1.65}$$

Actually, we can use for the spot size $w(z) \sim 2z/kw_0$, because the spot size is a hyperbolic function around $z = 0$, with the minimum w_0 at $z = 0$ and a, more or less, linear increase of the beam radius for large distances.
When z becomes very large $R \to z$ and the divergence angle is:

$$\theta_{beam} = \frac{w(z)}{R} = \frac{2}{kw_0} \tag{1.66}$$

It is useful to introduce a beam parameter called q, which is complex and defined as:

$$\frac{1}{q} = \frac{1}{R} - \frac{2i}{kw^2} \tag{1.67}$$

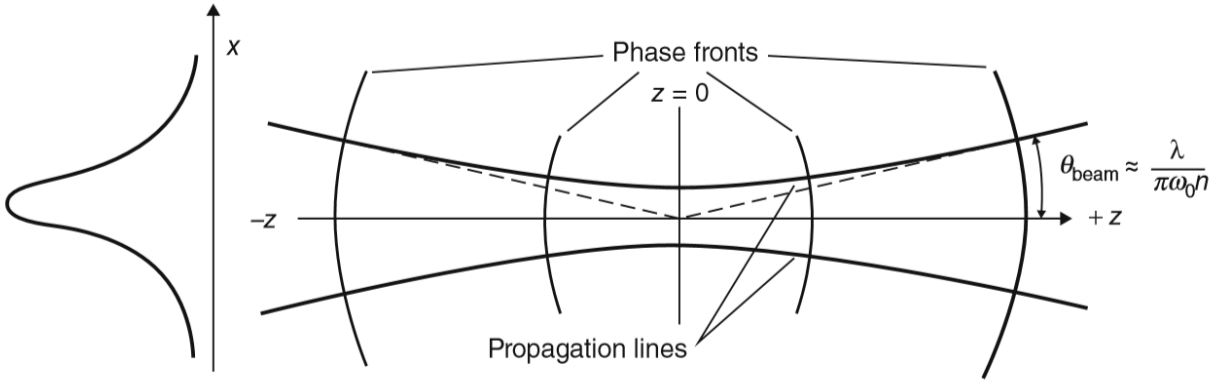

Figure 1.5: A representation of a Gaussian beam. On the left the transverse profile, on the right the shape of the beam as a function of z in the plane xz. From [8].

So, we can rewrite E in terms of q:

$$E = E_0 \left(\frac{w_0}{w}\right) \exp\left[\left(\frac{r^2\pi}{\lambda}\right)\left(\frac{1}{R} - \frac{i\lambda}{\pi w^2}\right)\right] \exp\left[-i(kz - \psi(z))\right] =$$

$$= E_0 \left(\frac{w_0}{w}\right) \exp\left[\left(\frac{r^2\pi}{\lambda}\right) q(z)\right] \exp\left[-i(kz - \psi(z))\right] \tag{1.68}$$

This parameter q is useful to see and study how a Gaussian beam changes when it traverses through an optical system (lens, mirrors, etc.).
There are other parameters relative to Gaussian beams, as the Rayleigh length, but as we will not use them, we will not describe them here in detail.
Note that Gaussian beams and planar waves are mathematical approximations. A real Gaussian beam has a Gaussian profile in all the axis, which means that a true Gaussian beam must have infinite energy, that is the reason why they are only approximations, but these approximations allows us to obtain good results.

Chapter 2

COMSOL Multyphysics

2.1 Overview

COMSOL is defined as a modeling and analysis tool for the virtual study of physics. COMSOL Multiphysics can model virtually any physical phenomenon that an engineer or scientist can describe with partial differential equations. The multiphysical capabilities integrated into COMSOL Multiphysics enable the user to simultaneously model any combination of phenomena. Thanks to these capabilities, it is possible to describe the model into 2 different ways, one through predefined applications that allow to create the model by fixing the physical quantity that characterize the problem, and the other, through the equations that model the problem, and it is also possible to combine both.
COMSOL facilitates the development of apps by having a lot of different libraries. All the different libraries is the reason that COMSOL is used in such different areas (Fig. 2.1). One of the most important areas in which COMSOL works are:

- Acoustics, electromagnetism, microelectromechanical systems (MEMS), microwave engineering, radio frequency components, semiconductor devices, wave propagation.
- Chemical reactions, diffusion, fluid dynamics, fluids in porous media, heat transfer, transport phenomena.
- Structure mechanics.
- General physics, geophysics, optics, photonics, quantum mechanics.
- Control systems.
- Component modeling.
- Applied mathematics.

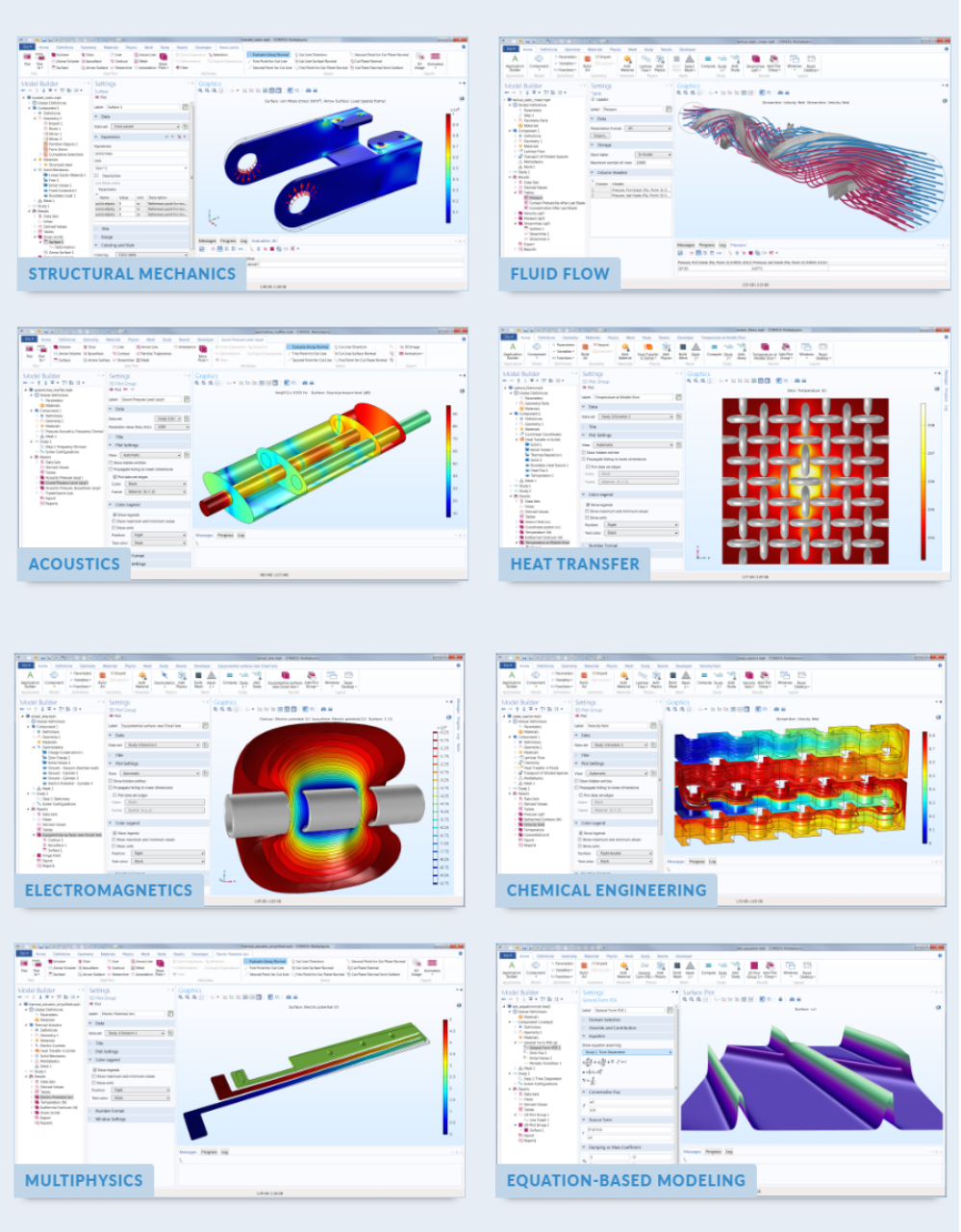

Figure 2.1: Some of the different fields in which COMSOL works.

Besides all this, there are some characteristics that makes COMSOL in a good election. First of all, COMSOL has a friendly and interactive graphic interface for all the modelling process, that is a very useful point, specially for new users. In addition, it is possible to simulate 1D, 2D and 3D systems, incorporating tools from CAD for a solid modeling in 1D, 2D and 3D. COMSOL is able to read files and import geometries from other programs like AutoCAD and CATIA. Another program compatible with COMSOL is MATLAB, with which COMSOL has a total integration whit it ant its toolboxes.

There are also some important characteristics about the processing. COMSOL has an auto-

matic and adaptive generation of meshes, with explicit and interactive control over their size. Controlling the mesh is a very important point, as we will show in Chapter 3. COMSOL also has the most newfangled solvers, including iterative solvers for seasonal linear and nonlinear problems, dependent on time, and eigenvalues. Post-processing is interactive, being able to visualize any function of the solution [14, 15].
Another interesting point for beginners are all the examples (more than 80) that explain all the features of COMSOL, e. g., related with optics, there are more than 5 examples which you can learn to simulate some basic problems, like simulate fresnel equations or simulate a Fabry Perot resonator[1].

2.2 COMSOL main interface

Having a friendly interface is a very important point, specially to attract and confirm new users, and COMSOL's interface meets these points. In each icon, if you place the cursor over it, it is given a brief description, which is always helpful for all users. In addition, with a very intuitive graphic interface and comfortable menu shortcuts, it seems that COMSOL is the correct option to our project.
COMSOL's interface is shown in Fig. 2.2. As we can see, it is possible to separate the interface in 3 different sections. The 3 divisions correspond to the toolbar, Fig. 2.2A, the model builder menu, Fig. 2.2B, and the Graphics section, Fig. 2.1C.
In next subsections, the 3 different menus of COMSOL will be explained in more detail. Due to the importance of seeing the interface well, it is displayed on the next page in landscape format.

[1] If one wants to use these examples, they are available at *File*, *Application Libraries*, *Wave Optics Module*, *Verification Examples*.

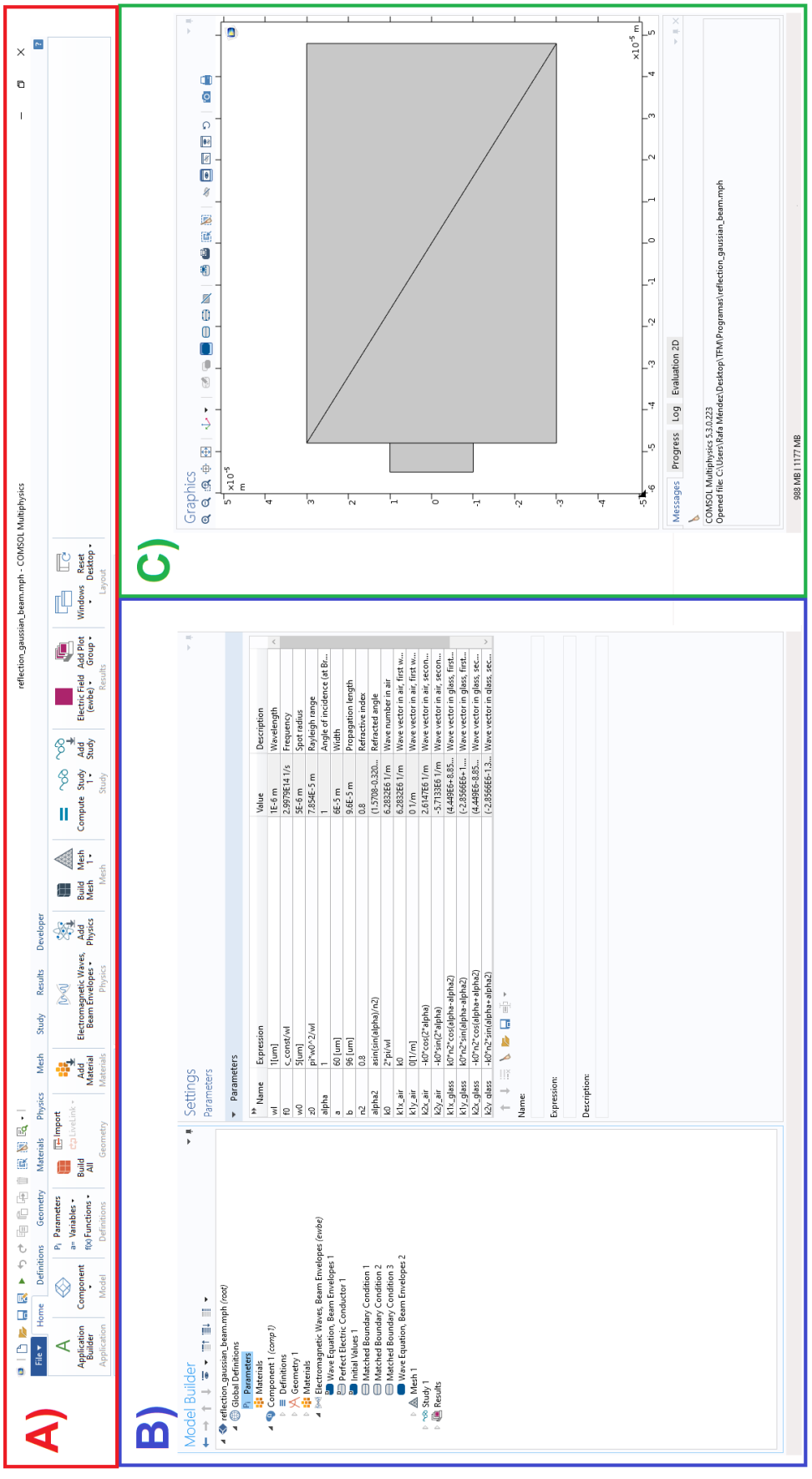

Figure 2.2: COMSOL's interface, with 3 different sections. A) represent the main toolbar, with all the different subsections to select the menus or add new elements and compute the program. B) is the model builder, where you can edit the values and definitions of the program. C) is the graphics menu, where the solution is displayed.

2.2.1 Toolbar A)

COMSOL's toolbar is like other programs toolbar, it is a graphical control element on which on-screen buttons, icons, menus, or other input and other output elements are placed. The toolbar allow us to select between the different menus to add or change elements to our model. There are 10 different sections inside the toolbar, each section with different subsections related with the section.
The sections are: File, Home, Definitions, Geometry, Materials, Physics, Mesh, Study, Results, Developer:

- File: by clicking it, it is shown the basic window that exits in every program, allowing us to create, load or save a file, and also to open the options, read the help, go to the applications libraries, etc.

- Home: home is, as the name suggests, the home section (Fig. 2.3), a quick access menu for the other sections.
  For example, the first option is the Application Builder, it open the Application Builder to modify the user interface of the application and to create and edit code for the application. Other options allow us to modify the geometry, define or edit parameters, add some physics, build the mesh, compute the program or visualize the results. All of these options are in their respective menus, but here we have a quick access to them.

- Definitions: in definitions we can add new parameters or formulas to our model or modify them. Here is where we define all the parameters that are needed for the model, e. g., in our model we define the wavelength and then the frequency as function of the wavelength.

- Geometry: in this menu (Fig. 2.4) there are some options to define graphically our model. Our program will be a 2D model, so the shapes that we will use are lines, circles and squares. It is also possible to join different parts, or measure the size of the objects.

- Materials: in materials we use the parameters in Definitions and the geometry defined in the previous section to define specifically the behaviour of the model. In our model we distinguish between air and glass.

- Physics: the physics section allows us to add the different physics that will be used in the model, here is where the different modules are loaded, in our model we will use the Electromagnetic Wave module in a Frequency Domain, but there are more different modules like Acoustic or Heat module. It is also possible to perform simulations with only one module, or multiple modules at the same time.

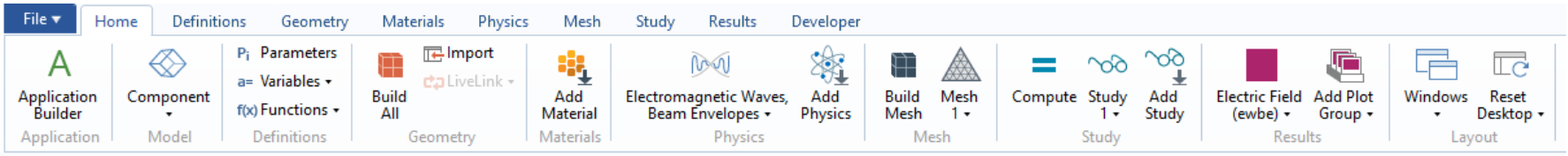

Figure 2.3: Home section, a quick access for the other menus.

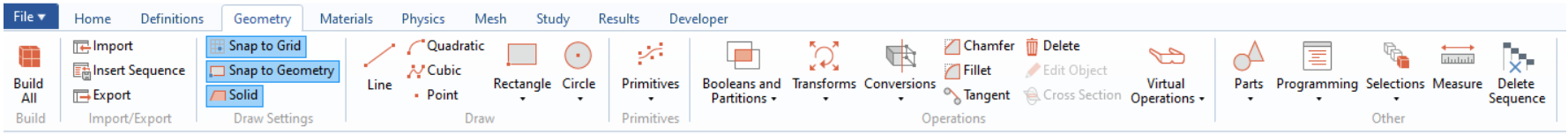

Figure 2.4: Geometry section, here you can define different geometries in different dimensions, depending on your model.

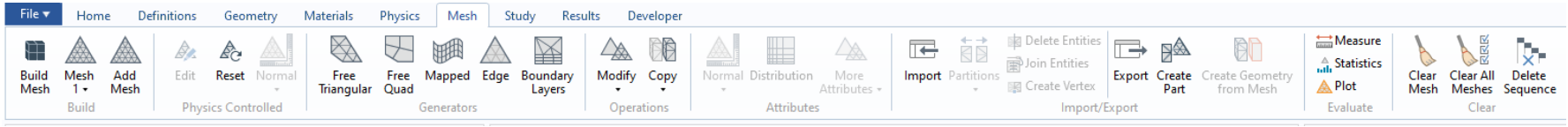

Figure 2.5: Mesh section, there are different types of mesh, here you add the mesh and build it.

- Mesh: this is one of the most important sections, here you define the mesh (Fig. 2.5), that is, the space or the points where the solver will realize its calculations. Having a good mesh is important to obtain correct results, generally, the finer the grid, the better the result obtained, but it requires more computational time and more power.

- Study: in this menu it is chosen the conditions for the study through the use of solvers. Solvers are defined depending on the way that we want the problem to be treated. The solver that we use will take the variables defined in Definitions, the initial conditions that we defined in Materials and Physics, the grid defined in Mesh and a Maxwell Equation FDTD solver to obtain the solutions to our problem.

- Results: here we define how we want our solutions to be shown, for example, to represent graphically the electric field on one axis and the position in another axis, or extract a line of magnetic field for a specific area and then export it as a data set to use it in a different program.

- Developer: Developer allow us to build an external application out of our model, with the capability to study it without using COMSOL.

2.2.2 Model builder menu B)

Model builder menu (Fig. 2.6) is a graphic menu where we can individually edit each parameter of our simulation.
It is possible to edit whatever you want: parameters, materials, variables, definitions, the geometry of the model, wave equations, boundary conditions, mesh, study and also edit the way to represent the results.
As an example, we can name the different variables and then edit their value or after drawing the geometry, we can assign to it the type of material we desire.

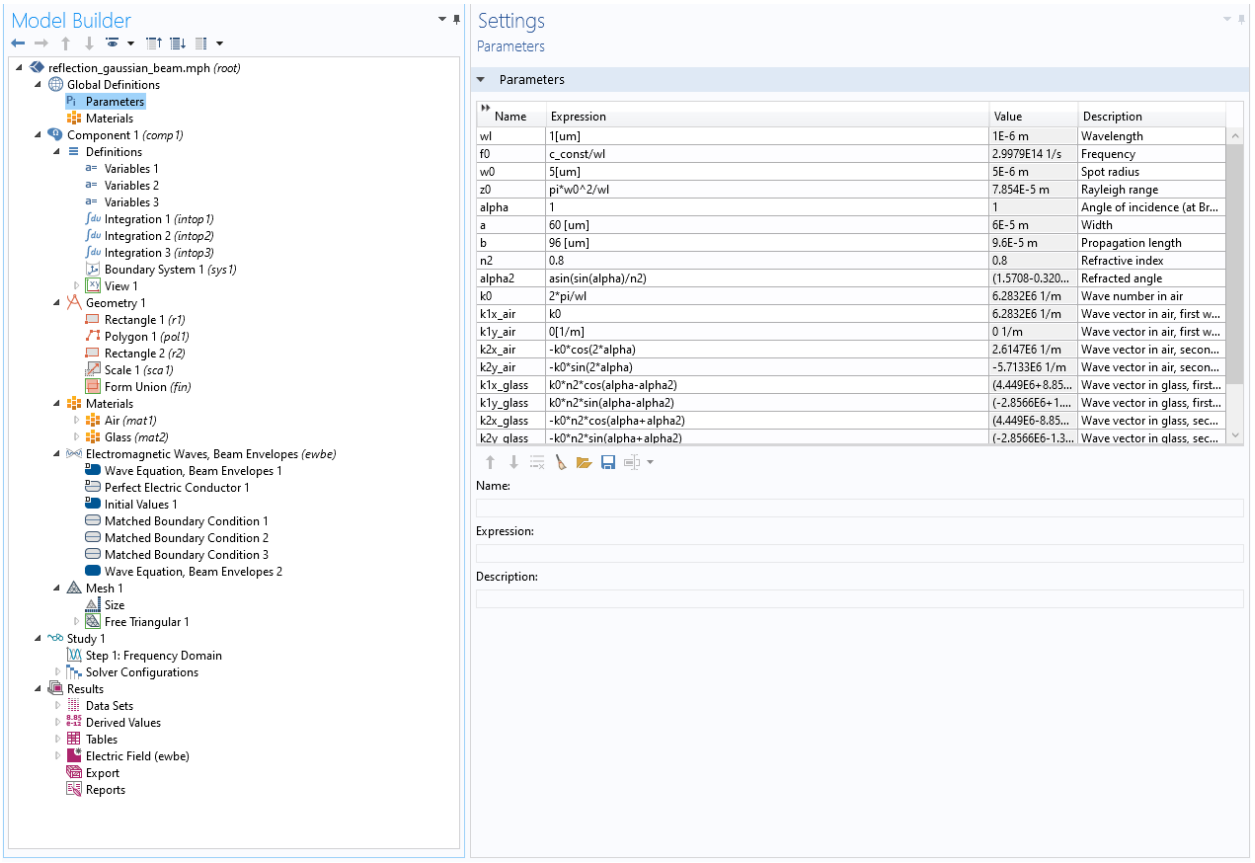

Figure 2.6: Model builder menu selected to edit the main parameters, but it is also possible to edit the geometry, the material, etc.

2.2.3 Graphics menu C)

This menu (Fig. 2.7) is used to graphically see the Results section, and also visualize other sections such as Mesh or Geometry, being also able to edit the geometry. It is also possible to analyze the convergence while the simulation is running to detect if there are problems in our model or the estimated error what might have in the calculations. At the bottom of Figure 2.7, there are some sub-menus, here is where we can analyze the simulation during the run.

Instead of selecting Results, in Figure 2.8 we are showing the grid, this is very useful to detect in which points the simulation is doing the calculations. For example, in the case of a specular reflection, we are not interested in having a fine mesh in the second material because the ray will not enter in it, so we can see how the grid is in the first medium to optimize it. To get the most accurate solutions, COMSOL bases its core in numerical methods. It realizes the study of PDE for stationary, time-dependent, frequency domain and eigenfrequency studies, discretizing by using the finite element method for the space directions. Also using boundary element methods to discretize such space, having a system of ordinary differential equations

which are solved using advanced implicit and explicit methods for time stepping.

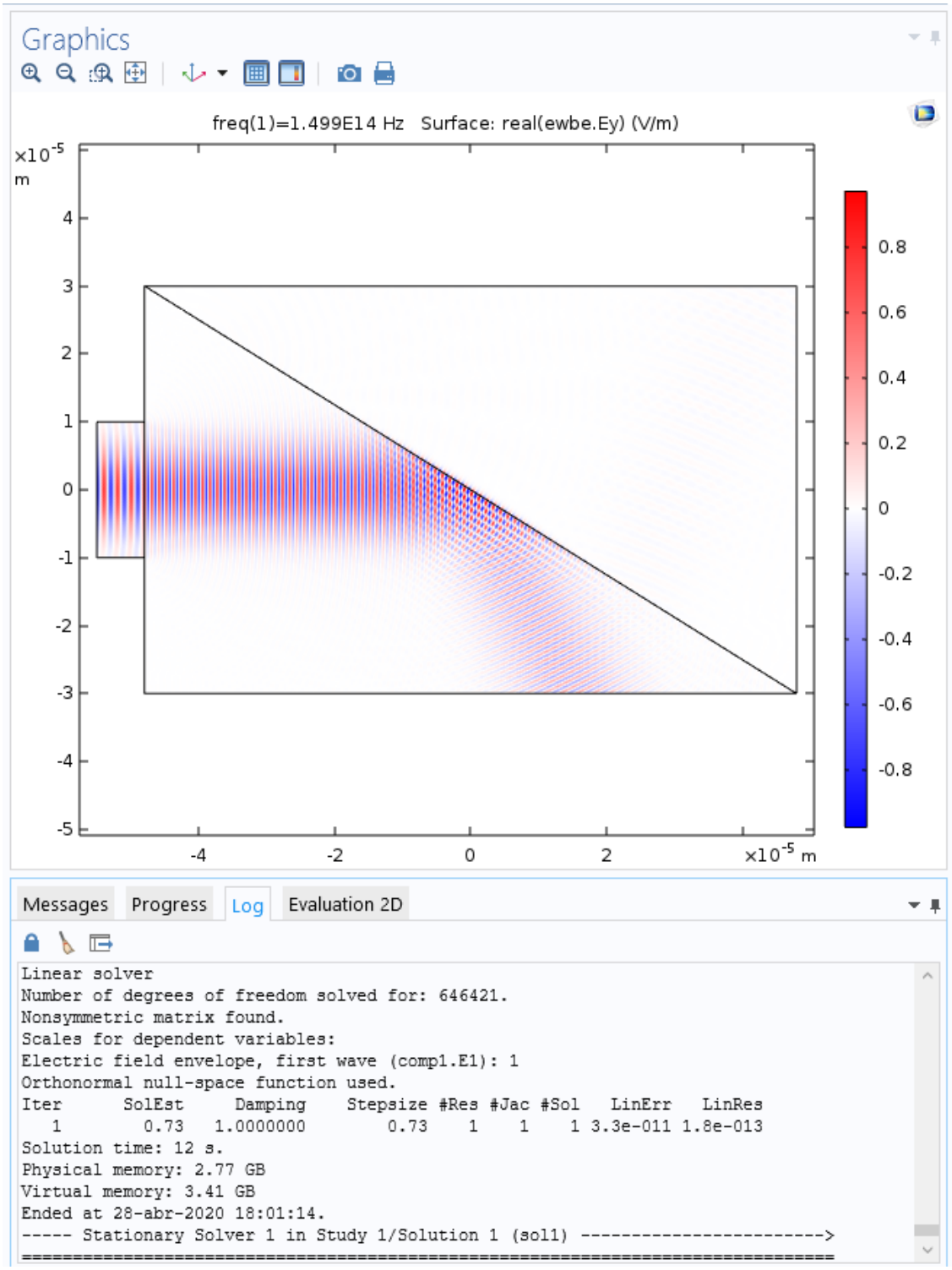

Figure 2.7: Graphics menu showing us the Results of the electric field.

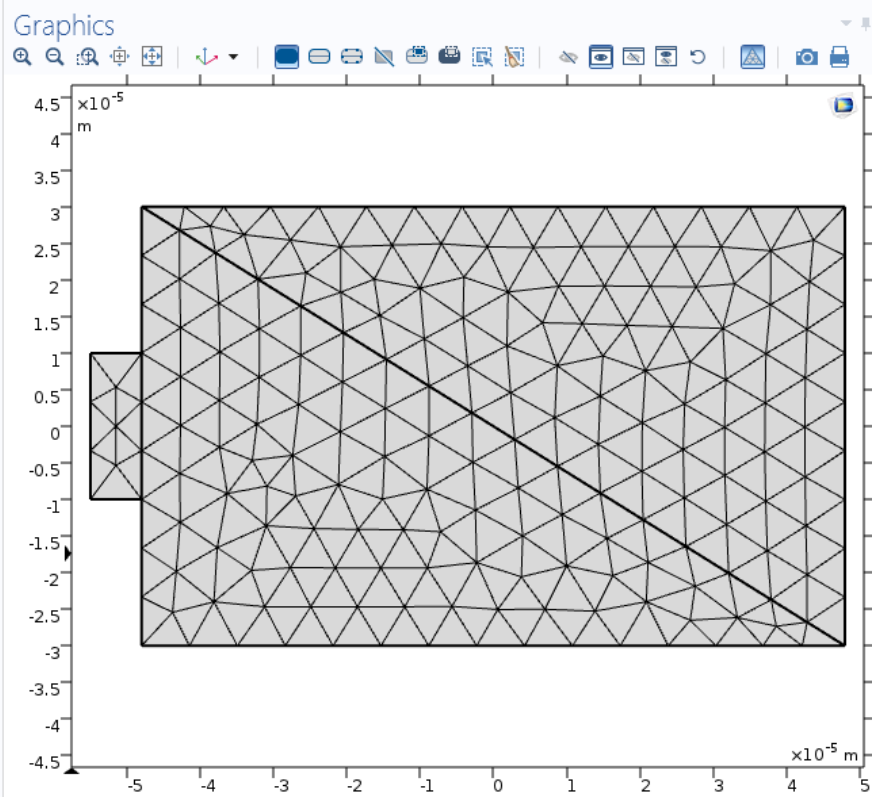

Figure 2.8: Graphics menu showing the Mesh. This is a predefined mesh as an example, very thick, and not useful for our simulations.

Our simulations in COMSOL will be solved by using the Finite-Difference Time-Domain method (FDTD).

2.2.4 Finite-Difference Time-Domain method (FDTD)

FDTD method, also known as Yee's method (Fig. 2.9), consist on a numerical analysis technique used for modeling computational electrodynamics, and it is one of the simplest numerical methods to implement. Furthermore, it is also a good approximation when solving Maxwell equations in spite of its simplicity. This method is used in a large number of simulations, but if the object is small compared to the wavelength of the problem it would be better to use quasi-static approximations. On the other hand, if the object is too large compared to the wavelength, it might be better to use ray-based methodology to solve it. FDTD belongs to finite difference methods where the time-dependent Maxwell's equations in partial differential form are discretized using central-difference approximations to the space and time partial derivatives. The resulting finite-difference equations are solved in either software or hardware in a leapfrog manner: the electric field vector components in a volume of space are solved at a given instant in time; then the magnetic field vector components in the same spatial volume are solved at the next instant in time; and the process is repeated

over and over again until the solutions satisfies the desired criteria.

FDTD method can be summarized in the next 5 steps:

1. All the Maxwell's equations in differential form are replace with finite differences, discretizing time and space, that means electric and magnetic fields are divided in time and space too.

2. The first iteration of the equations is solved, and then, there are obtained the new equations, that express the future fields based on the past fields.

3. Evaluate electric fields one time-step so the new values are known.

4. Evaluate magnetic fields one time-step so the new values are known.

5. The steps 3 and 4 are repeated until the solution satisfies a stop criteria.

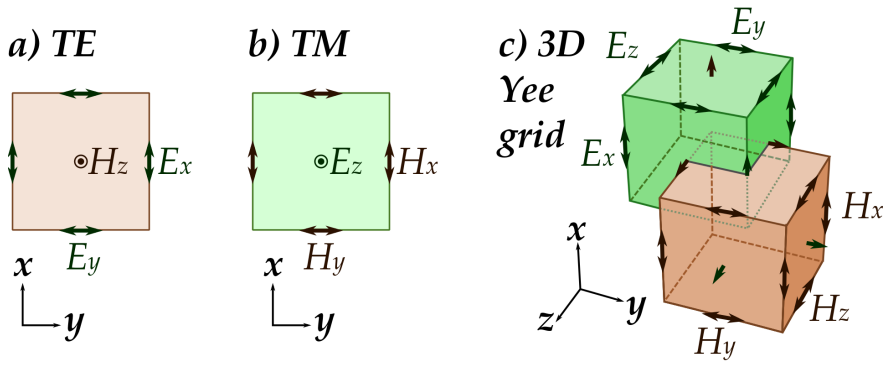

Figure 2.9: Illustration of how the finite-difference time-domain method in computational electromagnetism discretizes the space, interleaving the fields components for higher precision. For a system with translation symmetry along an axis, the TE/TM problems can be decoupled and solved separately. a) is a two-dimensional case with the magnetic field along the axis (perpendicular to the screen); b) is likewise a case with the electric field along the axis. In a general case, the Yee grid on figure c) is used. From [15]

Note that COMSOL makes all these calculations on its own, so that we only have to optimize those parameters related to the design of the experiment and the materials involved.

2.3 Our simulation in COMSOL

In this section we will describe the simulation that we will run and study. First, we are going to explain the different parameters used, and the geometry chosen. It will be also necessary to differentiate between 2 materials, glass and air. And one of the most important factors, as explained later, optimization of the mesh where the calculations will be carried

out by the software. Thus, we will describe in detail some of the features related to this process, and finally show the results obtained.

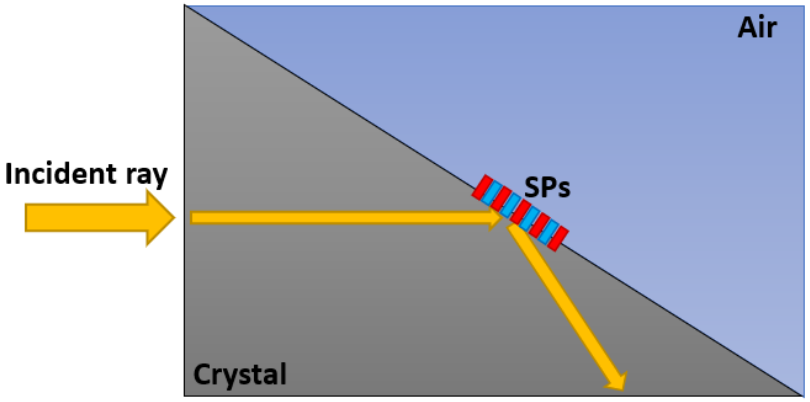

Figure 2.10: Sketch of our problem, there are 2 different media, in which a ray is reflected and SPs are created on the surface of a material.

The simulation will consist on an incident ray propagating in a specific medium (isotropic/uniaxial/biaxial), which suffers a reflection at the boundary of such medium with a dielectric (air). For simplicity, the ray is defined in air (in the biaxial medium it would be much more cumbersome), then it enters the crystal at normal incidence, and then it is incident on the crystal-dielectric boundary. Therefore, we need to define two different materials: the crystal and the dielectric. The sketch of the experiment is represented in Figure 2.10.

2.3.1 Modeling instructions

Creating a new file

From the **File menu**, we choose **New**. Then, in the new window, we click on **Model Wizard** where we select 2D, and in the physics tree, Optics>Wave Optics>Electromagnetics Waves, Beam Envelopes (ewbe). Until now, we have selected the Physics, the next step is to define the Study.
Clicking on study we open the study tree, here we choose frequency domain, and then we click done.

Global definitions

Settings

Parameters

Parameters

Name	Expression	Value	Description
wl	1[um]	1E-6 m	Wavelength
f0	c_const/wl	2.9979E14 1/s	Frequency
w0	5[um]	5E-6 m	Spot radius
z0	pi*w0^2/wl	7.854E-5 m	Rayleigh range
alpha	1	1	Angle of incidence (at Brewster angle)
a	60 [um]	6E-5 m	Width
b	96 [um]	9.6E-5 m	Propagation length
n2	0.8	0.8	Refractive index
alpha2	asin(sin(alpha)/n2)	(1.5708-0.32061i) rad	Refracted angle
k0	2*pi/wl	6.2832E6 1/m	Wave number in air
k1x_air	k0	6.2832E6 1/m	Wave vector in air, first wave, x component
k1y_air	0[1/m]	0 1/m	Wave vector in air, first wave, y component
k2x_air	-k0*cos(2*alpha)	2.6147E6 1/m	Wave vector in air, second wave, x component
k2y_air	-k0*sin(2*alpha)	-5.7133E6 1/m	Wave vector in air, second wave, y component
k1x_glass	k0*n2*cos(alpha-alpha2)	(4.449E6+8.8574E5i) 1/m	Wave vector in glass, first wave, x component
k1y_glass	k0*n2*sin(alpha-alpha2)	(-2.8566E6+1.3795E6i) 1/m	Wave vector in glass, first wave, y component
k2x_glass	-k0*n2*cos(alpha+alpha2)	(4.449E6-8.8574E5i) 1/m	Wave vector in glass, second wave, x component
k2y_glass	-k0*n2*sin(alpha+alpha2)	(-2.8566E6-1.3795E6i) 1/m	Wave vector in glass, second wave, y component

Name:

wl

Expression:

1[um]

Description:

Wavelength

Figure 2.11: Initial parameters that we introduced in our problem.

On the **Home** toolbar, we click on **Parameters**, which open the Parameters settings in the Model builder menu. In the table we introduce the parameters of Figure 2.11. These parameters can be modified, and some of them can be overwritten in the future, such as the refractive index if we want to modify the permittivity and properties of our crystal.

Geometry

We are going to define a geometry like that in Figure 2.10, so we need two rectangles, one of them smaller than the other, which will consist of air as the medium where the incident ray is created.

The larger rectangle is created on the **Geometry** toolbar by clicking **Primitives** and choosing **Rectangle**. In the settings window for Rectangle, we locate the **Size and Shape** section. In the **Width** text field, we type[2] a, as previously defined, and in the **Height** text field, we

[2]These parameters can change, they only represent the dimensions of the crystal.

type b.

There is also a line to be defined that separates the two media, air and the material considered. To define the line, we click **Primitives** and choose Polygon, and in the Settings window, we locate the Coordinates, defined by 2 vectors: $\mathbf{x} = -b/2\ b/2$ and $\mathbf{y}= a/2\ -a/2$. The definition of the line will depend on how much separation between materials we want and on the size of the rectangle.

As said, we also add another smaller rectangle, on the left of the first one, with the only purpose of generating the incident ray always coming from air. This rectangle is arbitrary, it can actually be defined inside the first rectangle or outside it, and we can also vary its dimensions. To create it, we proceed with the same steps as for the first rectangle, but choosing different dimensions and position vectors. For the dimension, we locate (again) the **Size and Shape** section, and in the **Width** text field, we introduce b/10, and for **Height** we introduce a/2. Then, we locate the **Position section** by typing x $=-b/2 + b/20$ and y =0. If we want the rectangle to be outside the first one, we type x $=-b/20 - b/2$ and y =0. As said, there will be no difference between locating the smaller rectangle outside or inside the material, its only purpose is to generate the incident ray in air (defining the incident ray in other media could be more complicated, especially for biaxial media). In the following results, we will always place the rectangle inside the material for convenience, so we can slightly reduce the cost of meshing time. The results of this section are shown in Figure 2.12.

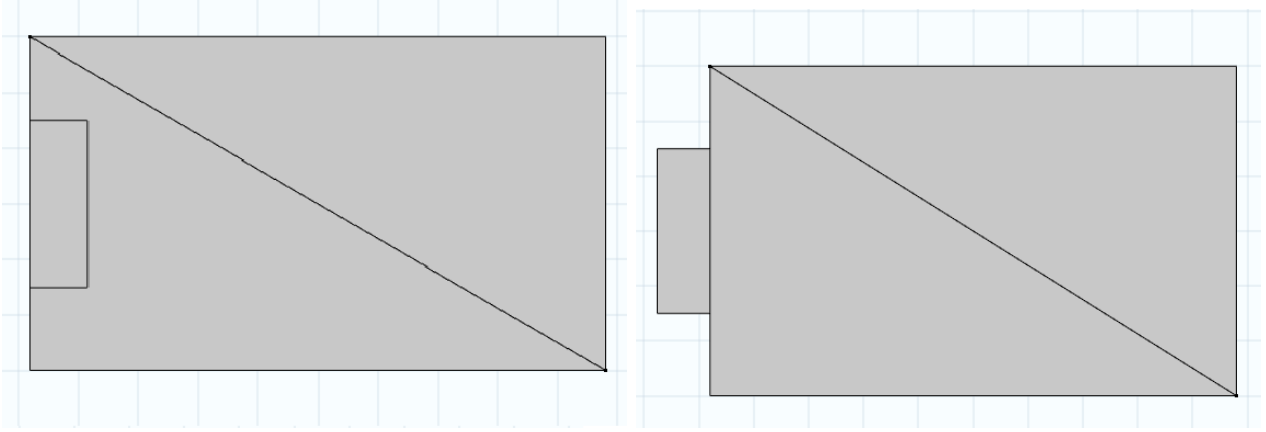

(a) Rectangle (where the incident wave is generated) "inside" the crystal.

(b) Rectangle (where the incident wave is generated) outside the crystal.

Figure 2.12: Both systems are equivalent

Materials

In the **Model Builder** window, under **Component 1**, we right-click **Materials** and choose **Blank Material**. In the **Settings** window for Material, we type Air in the **Label**

text field. Then, we locate the **Materials Contents** section and enter the parameters from Figure 2.13:

Material Contents

Property	Name	Value	Unit	Property group
Relative permittivity	epsilonr	1	1	Basic
Relative permeability	mur	1	1	Basic
Dynamic viscosity	mu	eta(T[1/K])[Pa*s]	Pa·s	Basic
Ratio of specific heats	gamma	1.4	1	Basic
Electrical conductivity	sigma	0[S/m]	S/m	Basic
Heat capacity at constant pressure	Cp	Cp(T[1/K])[J/(kg*K)]	J/(kg·K)	Basic
Density	rho	rho(pA[1/Pa],T[1/K])[kg/m^3]	kg/m³	Basic
Thermal conductivity	k	k(T[1/K])[W/(m*K)]	W/(m·K)	Basic
Speed of sound	c	cs(T[1/K])[m/s]	m/s	Basic
Refractive index, real part	n	1	1	Refractive index
Refractive index, imaginary part	ki	0	1	Refractive index

Figure 2.13: Parameters for air material.

We have also to define which domains correspond to each material[3]. In this case, we localize the **Geometric Entity Selection** section, and, for air, we add domains 2 and 3.
For defining the crystal material, the procedure is the same, in the **Model Builder** window, under **Component 1**, we right-click **Materials** and choose **Blank Material**. In the **Settings** window for **Material**, we type Glass in the **Label** text field. And, again, we locate the **Materials Contents** section and enter the parameters from Figure 2.14:

Material Contents

Property	Name	Value	Unit	Property group
Relative permeability	mur	1	1	Basic
Electrical conductivity	sigma	0	S/m	Basic
Relative permittivity	epsilonr	eps2	1	Basic
Refractive index, real part	n	n2	1	Refractive index
Refractive index, imaginary part	ki	0	1	Refractive index

Figure 2.14: Parameters for glass material.

For the glass material, in the **Geometric Entity Selection** section we add domain 1.

Electromagnetic Waves, Beam Envelopes (ewbe)

In the **Model Builder** window, under **Component 1 (comp 1)**, we localize and click on **Electromagnetic Waves, Beam Envelopes (ewbe)**. In the **Settings** window, we look for the **Components** section and, from the **Electric field components solved for** list, we select Three-component vector.
Now, we have to define the boundaries, domains and initial values:

[3]By default, the first material that added is applied on all domains

- On the **Physics** toolbar, we click **Domains** and select **Wave Equation, Beam Envelopes**. Here, we are going to define some electromagnetic parameters.
  We click on **Wave Equation, Beam Envelopes 1**, localize **Domain Selection** section, and add domains 2 and 3. Now, we locate **Electric Displacement Field**, and from the **electric displacement field model** list we select Relative permittivity. In the **Magnetic Field** section, we locate the **Relative permeability** list, and choose **User defined**, this parameter should be 1. Finally, we locate **Conduction Current** section, and in the **Electrical conductivity** list, we choose **User defined**, which must be 0.

- We now go to the **Physics** toolbar, click **Domains** and select **Wave Equation, Beam Envelopes**.
  We click **Wave Equation, Beam Envelopes 2**, first, and add domain 1 in the **Domain Selection**. We locate **Electric Displacement Field**, and from the **electric displacement field model** list we select Relative permittivity. Instead of using the permittivity from the material, we are going to select it in the **Relative permittivity** list **User defined**. Here we can define a uniaxial/biaxial material using a diagonal tensor for the permittivity.
  For the **Magnetic Field** section and **Conduction Current** section we repeat the previous step.

- We now go again to the **Physics** toolbar, we click on **Boundaries** and select **Initial Values**. On the **Model Builder** menu, under **Wave Equation, Beam Envelopes (ewbe)**, we select **Initial Values 1**, and in the **Domain Selection** section we add all the domains, i.e. 1, 2 and 3.

- Now, we have to define the boundaries, on the **Physics** toolbar. To do that, we click on **Boundaries** and select **Perfect Electric Conductor**. On the **Model Builder** menu, under **Wave Equation, Beam Envelopes (ewbe)**, we select **Perfect Electric Conductor 1**, and, in the **Boundary Selection** section we include boundaries 1 and 5.

- It is time now to create the incident pulse. On the **Physics** toolbar, we click on **Boundaries** and select **Matched Boundary Condition**. On the **Model Builder** menu, under **Wave Equation, Beam Envelopes (ewbe)**, we select **Matched Boundary Condition 1**.
  In the **Settings** menu, we add boundary 3 in the **Boundary Selection** section. Then, we locate the **Matched Boundary Condition**, and under the **Incident electric field envelope**, for the **y** component, we type $exp(-(y/w0)^2) * 1$.

We have defined a Gaussian pulse, that is launched in boundary 3, which corresponds to the small rectangle (air).

- We now on the **Physics** toolbar, click on **Boundaries** and select **Matched Boundary Condition**. On the **Model Builder** menu, under **Wave Equation, Beam Envelopes (ewbe)**, we select **Matched Boundary Condition 2**. In the **Settings** menu, we locate the **Boundary Selection** section, and add boundary 2.

- Finally, on the **Physics** toolbar, we click on **Boundaries** and select **Matched Boundary Condition**. On the **Model Builder** menu, under **Wave Equation, Beam Envelopes (ewbe)**, we select **Matched Boundary Condition 2**. In the **Settings** menu, we locate the **Boundary Selection** section, and add boundaries 8 and 10.

Mesh

In the **Model Builder** menu, under **Component 1 (comp 1)**, we right-click on **Mesh 1** and choose **Free Triangular**. There are more options, for example, using a Free Quad. In the next section we will explain why the Free Triangular is better than others for our particular case.
Under **Mesh 1**, we right-click **Free Triangular 1**, and click **Size**. The purpose of this step is to define a finer mesh for the areas where the calculations are carried out. For air, the area where the pulse never goes through, we do not need a very fine mesh (which would cost more computational power), so we define a different thicker mesh.
To do this, under **Free Triangular 1**, we click **Size 1**. We localize the **Geometric Entity Selection** section, and add domains 1 and 2. We locate **Element Size** and select **Custom**. Finally, we localize **Element Size Parameters**, select **Maximum element size** and type $wl/7$.
The grid will depend on the wavelength, the smaller the wavelength the finer the mesh should be. Indeed, the mesh can be set arbitrarily small depending on the computing capability.
For the mesh in air, we proceed as in the previous step: under **Mesh 1**, we right-click **Free Triangular 1**, and click **Size**. Click **Size 2**. We localize the **Geometric Entity Selection** section, and add domain 3. We locate **Element Size** and select **Custom**. Finally, in **Element Size Parameters**, we select **Maximum element size** and type $wl/5$.

Study

On the **Home** toolbar, we click **Compute** and see the results.

NOTES:

1. The selected parameters are defined for a default biaxial hyperbolic system, in the next Chapter we will choose different parameters to simulate different material conditions (isotropic, elliptical and hyperbolic). We will comment which parameters are changed and their new values. It is also possible to use other parameters, but you should take into account that different parameters mean different conditions and the result could show a poor resolution, so the idea is to find an optimal set of parameters and thus optimal results.

2. The following results will be performed with light instead of SPs due to the simplification of the problem (specially when exciting the incident wave), however, all results can be extrapolated to SPs. Furthermore, in the hyperbolic case it is possible to observe SPs that emerge on the boundary.

Chapter 3

Numerical simulations

In this chapter we are going to show the results of the simulations and discuss about them. The first result that we found in the simulation procedure is the importance of the mesh, so this will be our starting point. Then, once we have achieved a good mesh, the second point is to simulate reflections in different materials to study the differences obtained depending on the material properties.

3.1 The importance of the mesh

As seen in the previous chapter, there are different types of mesh, triangular, quad, etc. We start selecting a free triangular mesh, but, as we show in Figure 3.1 this type of mesh is not optimal.

The mesh suffers a crowding in the middle of each geometry, the crowding in the right part is not important, because the light never refracts. The main problem is for the left part, where the light goes through, so the mesh should be well defined because it will defined the points where the program will realize the calculations. However, it exists a kind of agglomerated grid, a discontinuity, so the mesh is not constant.

For the simplest case (isotropic material) the given solution is correct, but when the calculations became more difficult, for example, when the medium is biaxial, it leads into background noise, as shown in Figure 3.3.

In this case, the solution is not that bad, because one can correctly identify the expected reflection process, however there is background noise. This noise could be improve in some ways, but also it could be even worse, as we are going to show below. In Figure 3.2 are shown two images, in Figure 3.2a we have change some values of the permittivity, particularly, we have chosen a biaxial medium with negative refraction index in 2 different directions, such that the calculations need to be more accurate, but the current mesh is not fine enough, so

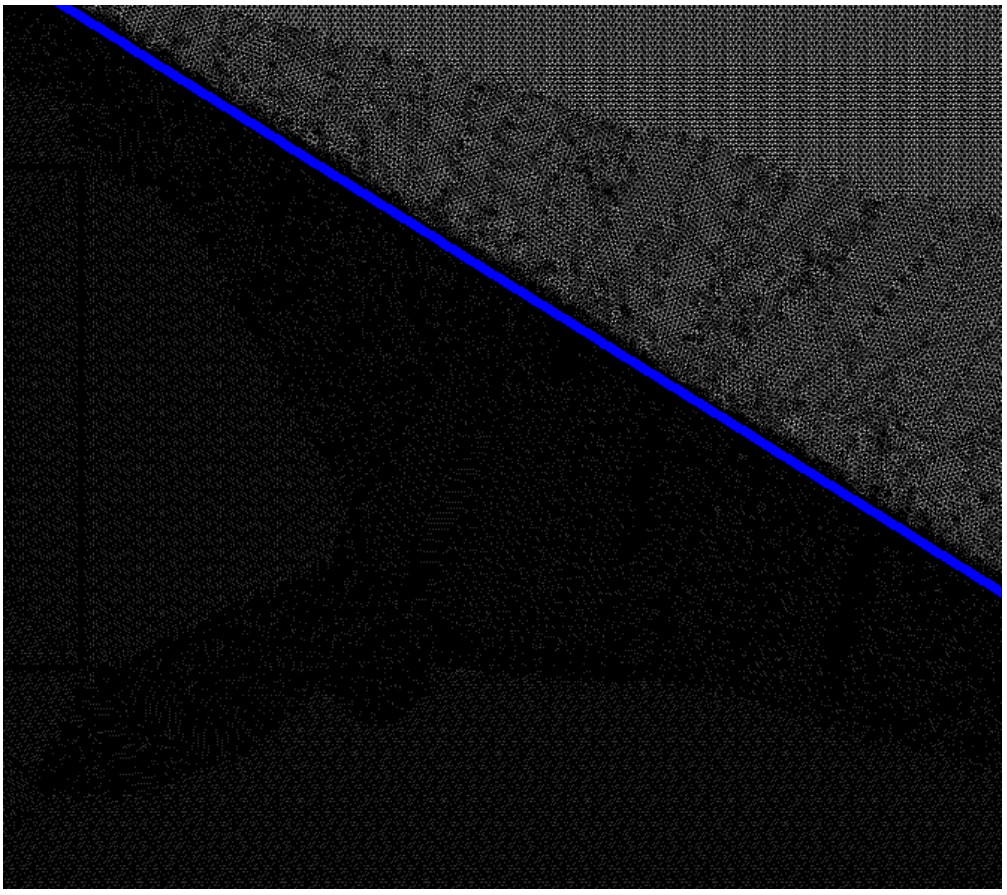

Figure 3.1: Initial mesh, it lacks of a grid continuity.

it results in a lot of background noise. If we compare both Figure 3.2a and Figure 3.1, the noise concentrates at the discontinuities in the grid.

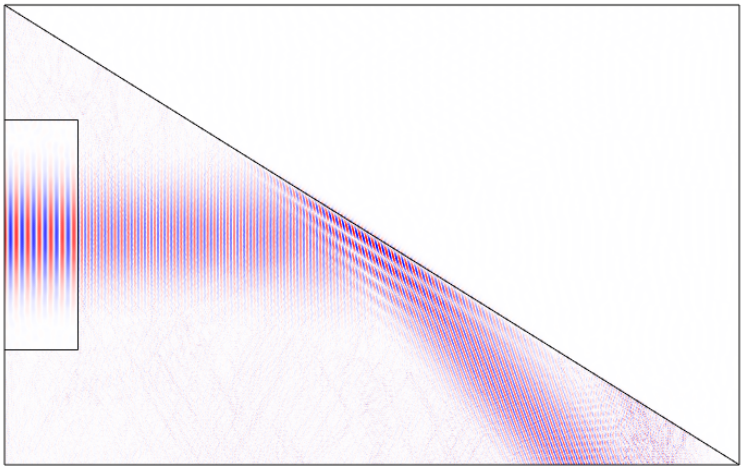

Figure 3.3: Solution for a biaxial medium, where some noise is generated due to the mesh.

In Figure 3.2b, instead of changing the permittivity, we have decreased the mesh size. The

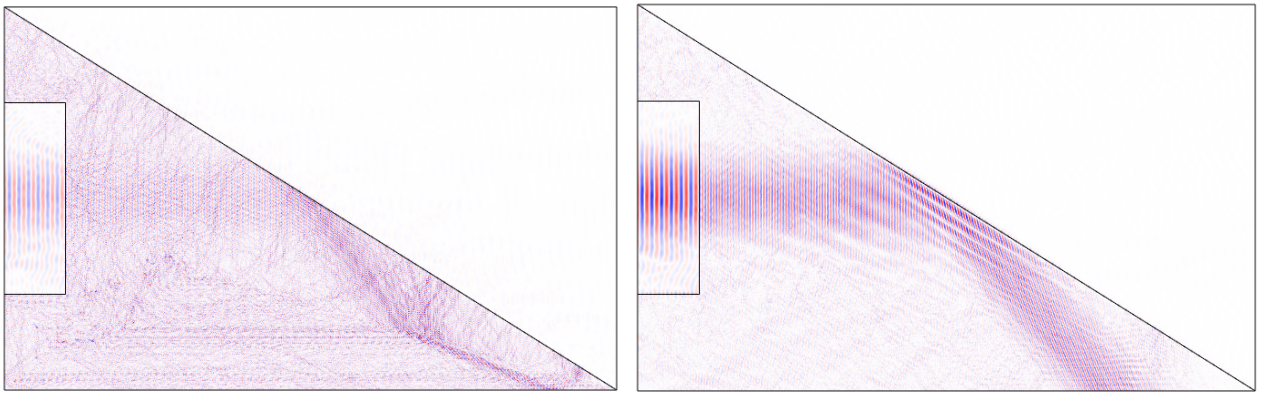

(a) Extreme case, with determined parameters to bring on background noise.

(b) In this example, instead of changing the parameters, the mesh is made bigger, so the results are poorer.

Figure 3.2: Examples of how a bad mesh can lead into wrong results.

result is the same solution as in Figure 3.3, but with more background noise.
There are some tricks to improve the mesh, the most basic and obvious is to reduce the grid size, having a finer mesh means to have more points where to carry out the calculations reducing the discontinuity, but it will also require more computational power.
Within all mesh types we have try in this work all of them (the most typical are triangular and quad) and the best solution was obtained for the free triangular mesh, where the grid is made up by triangles. To decide which mesh type was better we took care of the geometry taking into account that for a rectangle the best mesh is a free quad mesh. However, in this case, in which we separate the system into two triangles and one rectangle, the best way to optimize the grid is using a free triangular mesh. But, why is this happening?.
First point, let us compare the use of a triangular or quad mesh in this system. To do that, we define the grids, one made with a free triangular mesh, and the other with a free quad mesh. Both will be defined with the same parameters, only changing the mesh type. The chosen parameters are for the **Maximum element size**, as is Chapter 3, typing $wl/5$ for domains 1 and 2 (the crystal and the small rectangle) and $wl/3$ for domain 3 (air)[1].

[1]The parameters given in Chapter 3 were $wl/7$ and $wl/5$ but as this is only to demonstrate how the mesh works we decided to reduce the mesh size a bit.

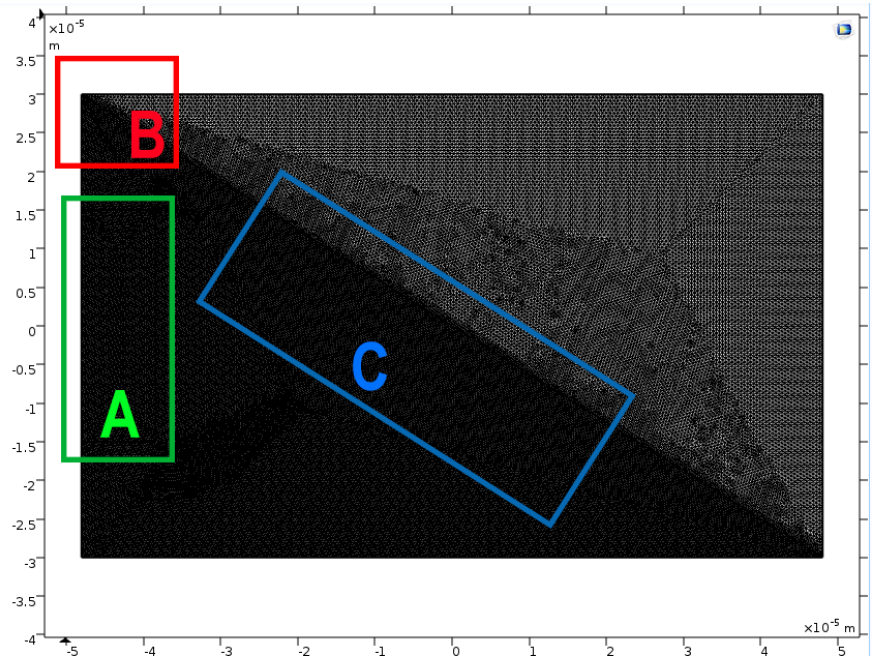

(a) System with a Free Triangular Mesh.

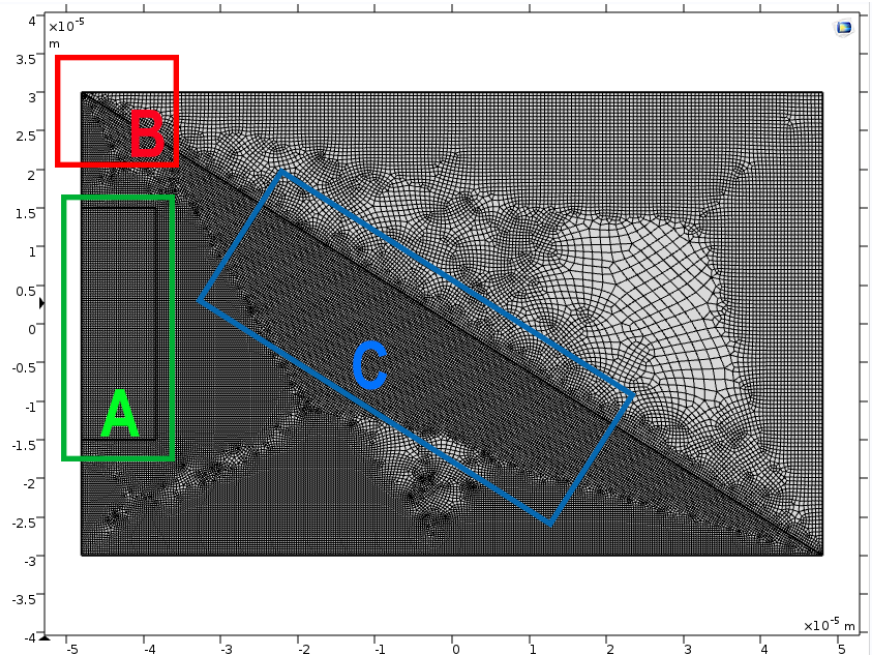

(b) System with a Free Quad Mesh.

Figure 3.4: System to solve when comparing two different mesh types. To discuss them we marked 3 different areas. In A we compare the rectangle where the light is generated, in B we discuss about the mesh in the corner, and in C we compare the center of the system.

At first glance (Fig. 3.4), it looks obvious that the triangular mesh generates a more regular and finer grid than the free quad grid mesh. But paying attention to areas A, B and C, we can observe in a better way why a triangular mesh is better in this case:

- Section A:
  In section A we are zooming to the place where the incident pulse is generated, it is represented in Figure 3.5, there are more parts besides the rectangle, but now we are going to only take the small rectangle into account.

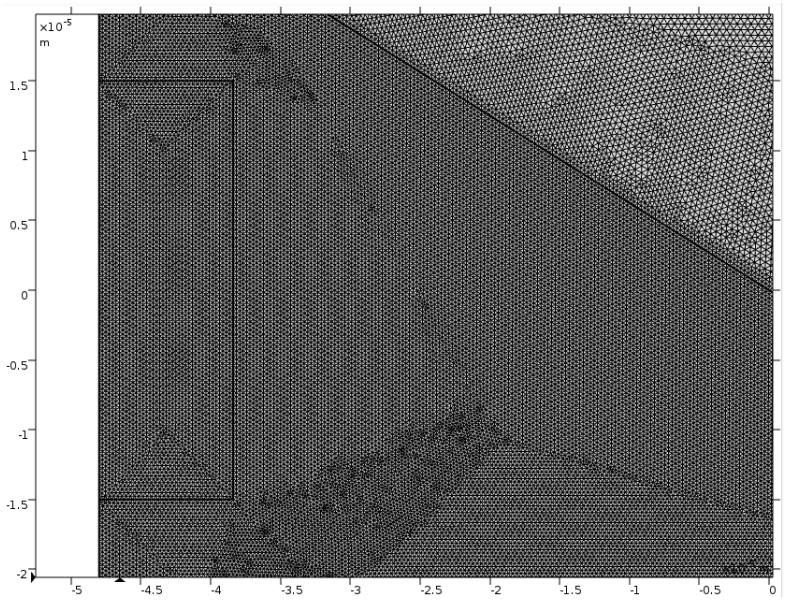

(a) Triangular mesh. Section A. Zoom to the small rectangle.

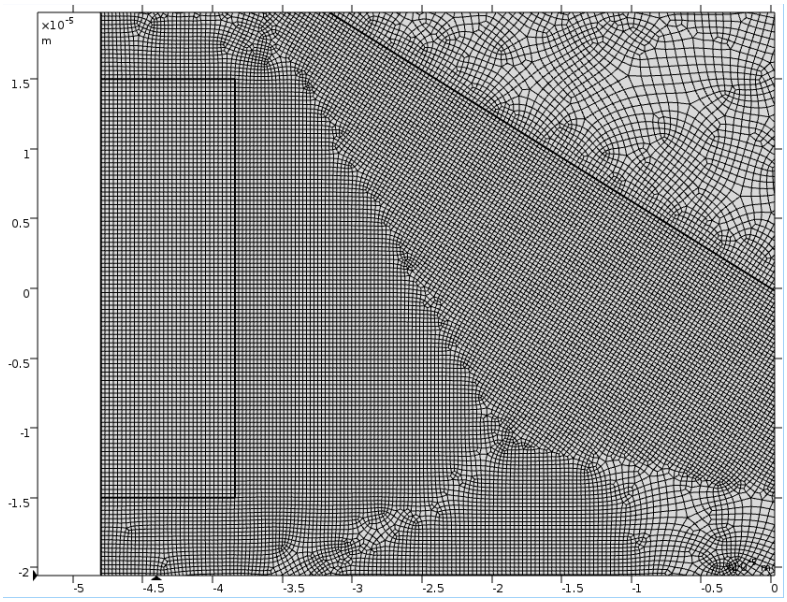

(b) Quad mesh. Section A. Zoom to the small rectangle.

Figure 3.5: Comparison between triangular and quad mesh. Section A from Figure 3.4.

In Figure 3.5b it is shown how this part results with a quad mesh, as the geometry corresponds to a rectangle, meaning that a quad mesh can fit better to it.
In the other hand, in Figure 3.5a it is shown the same rectangle but with a triangular

mesh. The result is that here a free quad mesh is better, it is continuous in the entire rectangle, however, the free triangular mesh has 2 small discontinuities above and below the rectangle, with a triangular shape.

- Section B:
  Section B corresponds to the upper left corner of the crystal (Fig. 3.6).

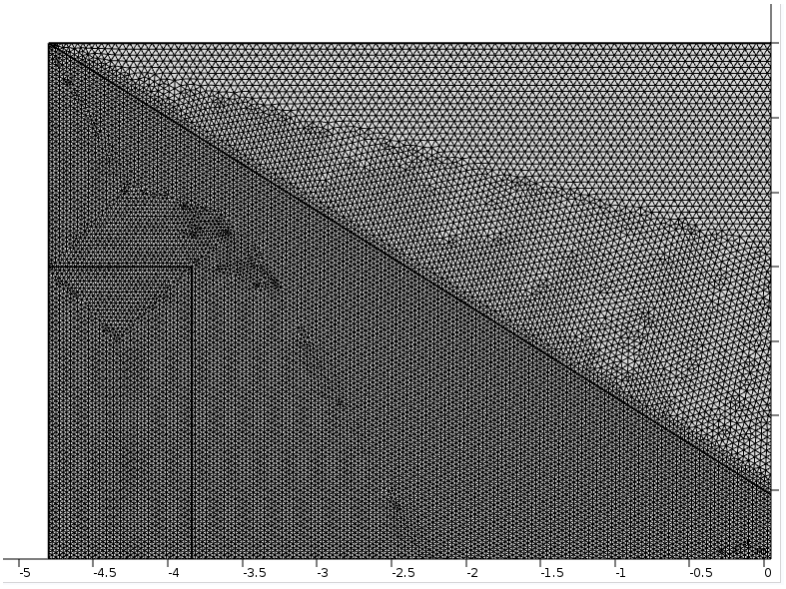

(a) Triangular mesh. Section B. Zoom to the upper left corner.

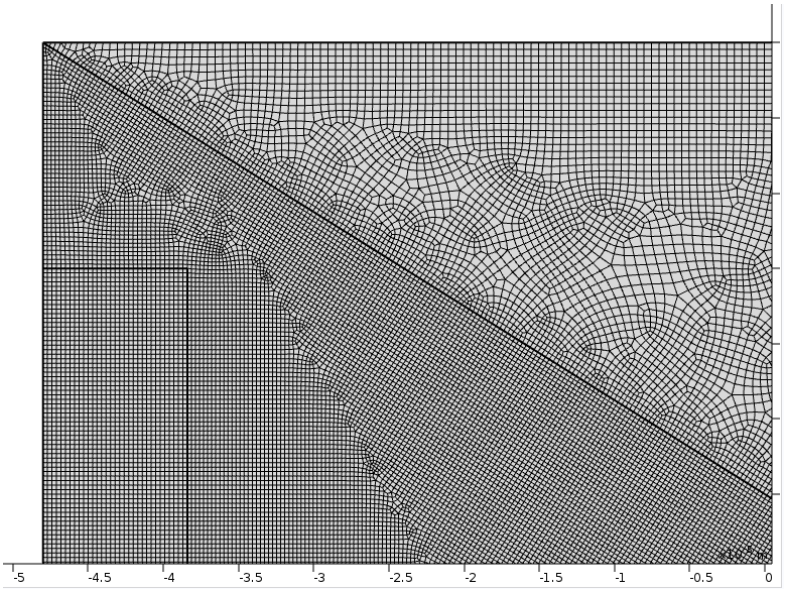

(b) Quad mesh. Section B. Zoom to the upper left corner.

Figure 3.6: Comparison between triangular and quad mesh. Section B from Figure 3.4.

In this part of the system (the corner), a triangular grid seems to fit much better than a quad grid. This is because the corner corresponds to a triangle, so it is impossible

to define it properly with square shapes.

It is also very difficult to have a perfect triangle grid in all the simulating area, as a discontinuity that starts from the middle of the corner propagates along the material. Both meshes show this discontinuity, but it is more noticeable for the quad mesh case.

- Section C:

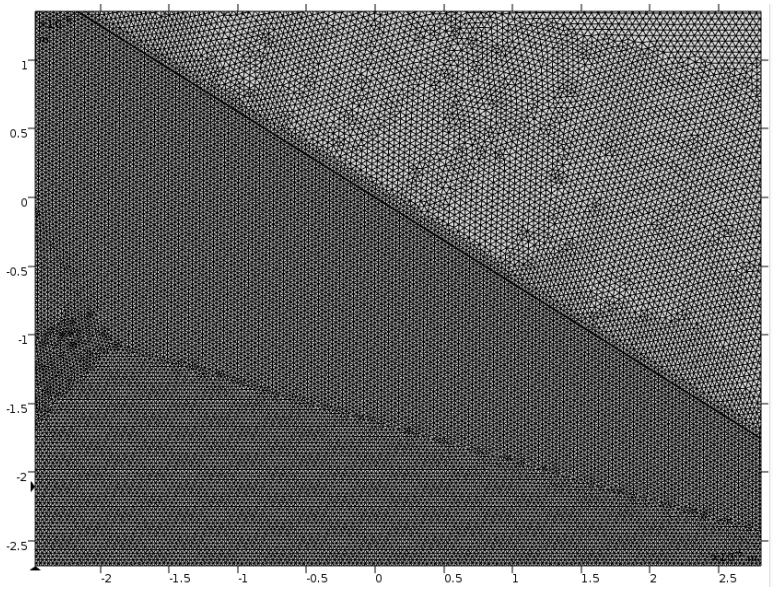

(a) Triangular mesh. Section C. Zoom to the center of the system.

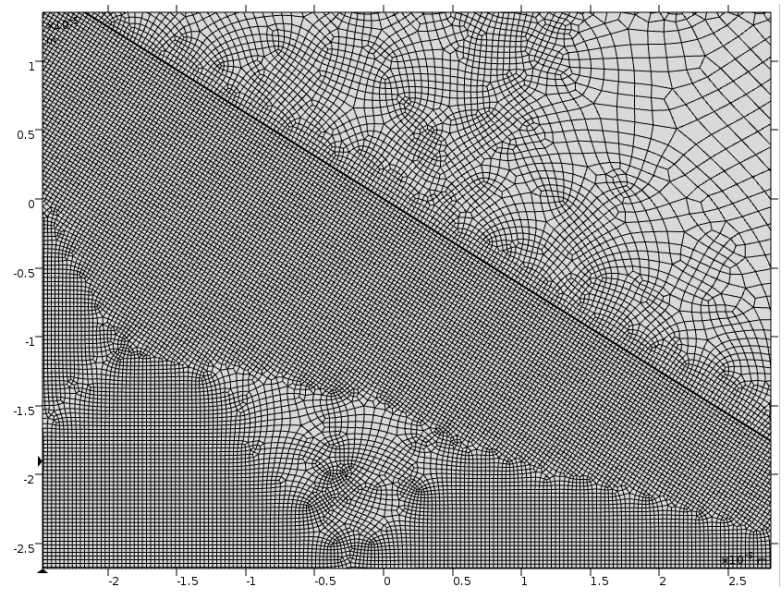

(b) Quad mesh. Section C. Zoom to the center of the system.

Figure 3.7: Comparison between triangular and quad mesh. Section C from Figure 3.4.

This section, Fig 3.7, represents the center of the system, with a very important bound-

ary between the crystal and air. It is also a boundary between a fine grid and a larger grid.

Here is interesting to notice that the discontinuity that started in the corner has spread through the system and have induced a big discontinuity in the middle, specially for the quad mesh. This is the most important area of the physics evaluation in our particular problem, so it is necessary to obtain an optimal mesh.

Another reason to explain why this happens is due to the boundary conditions. In COMSOL, when there are 2 different geometries next to each other, it is necessary to create boundary conditions between them. For example, when a pulse goes from a material to another it always goes through a boundary, so the program must have a well defined grid to calculate the path of the pulse. The way to implement this is with a boundary such that the entire grid from one side must match with the other side grid.

In the center of our system, we have a triangular grid in one side that has smaller elements than the grid of the other side, so, only near the border, where the grid is larger, there are the same number of triangles in both sides, this is represented in Figure 3.8. The crystal part has a finer mesh, in the boundary COMSOL creates the same number of calculation points in one side than in the other. In the air side, the grid suffers a change and acquires a more convenient geometry.

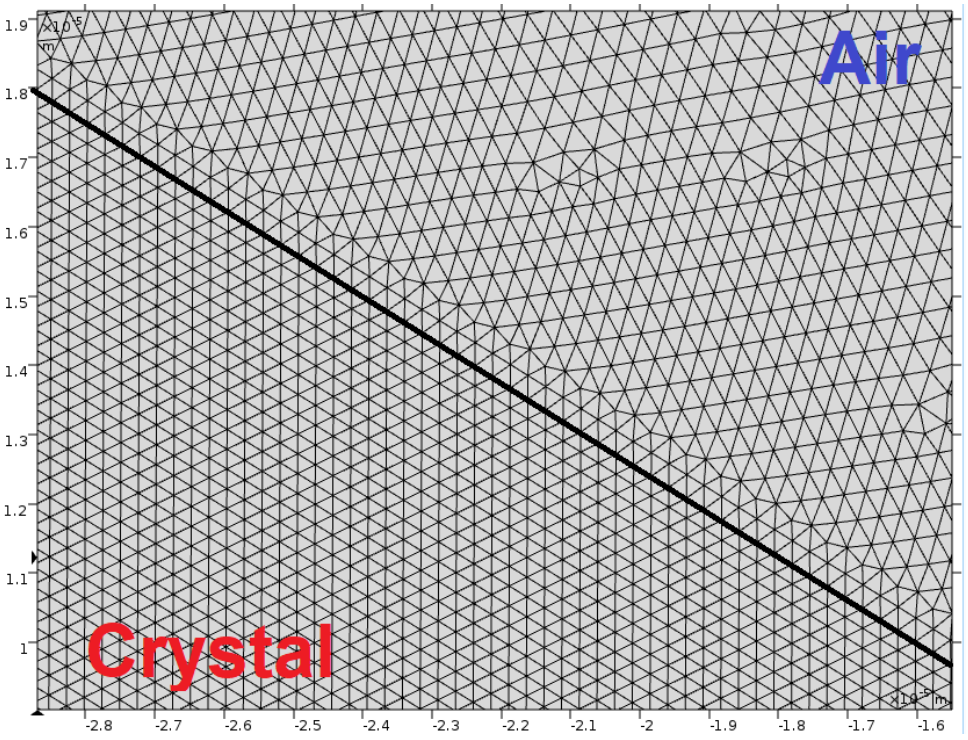

Figure 3.8: Boundary between crystal and air (center of the system, section C). The border is highlighted with a black line.

In summary, at the corner the triangle grid fits better, nonetheless it is always generated a discontinuity which propagates along the material. The discontinuity is due to the need to perfectly match the boundaries and the differences between the geometries. However, if the mesh is fine enough we can obtain good results without any problem.
It is also important to notice that the background noise problem only occurs when the calculations are complicated (negative refractive index), because the program needs to be more accurate.

3.2 Reflections in different materials

In this section we are going to simulate the reflection of light in 3 types of materials, with the purpose to excite SPPs/SPhPs in VdW biaxial materials. To do that, first we will define a Gaussian pulse, defined by a Gaussian function.

Particularly, the 3 different systems that we will consider are:

- Isotropic: this is the most common case, which should show a typical specular reflection, where the incidence angle is the same than the reflection angle. Here, as we have said, the energy will go in the same direction than the wavevector.

- Elliptic material: in this case the reflection angle will change with respect to the incidence angle. Depending on the material (the permittivity function in all three directions of space) the reflection angle will be different. The direction between the Poynting vector and the wavevector will generally be different. The elliptic materials that we simulate will be all uniaxial.

- Hyperbolic material: here we have the most uncommon case. The reflection angle could be very different compared with the incidence angle, this is what is called as hyperbolic reflection, where one (or two) optical directions of the material behaves as a metal. In very particular case, can occur that the reflection angle is negative (anomalous reflection) or even the wave comes back overlapping the incident one (backreflection). The Poynting vector and the wavenumber will have different directions.

When talking about a pedagogical reflection problem the solution is given by the typical form of the Snell's law, where the incidence angle is the same as the reflection angle. However, this condition is only true in isotropic materials (where n is constant and equal in all three directions of space), when using anisotropic materials we will need to use a more generic and difficult equation. Actually, the condition that must be satisfied is the momentum

conservation given in Eq. (3.1), and the most basic Snell's law comes from this condition. To explain this we can take into account the isofrequency curve for each case.

$$\Delta\vec{k} = \vec{k_i} - \vec{k_r} = 0 \tag{3.1}$$

Let us assume a isofrequency curve $f(k_x,\ k_y)$, with the normalized incident and reflected Poynting vectors $\vec{S_i}$ and $\vec{S_r}$, and the normalized wavevectors $\vec{k_i}$ and $\vec{k_r}$ for the incident and reflected ray respectively. The incident ray impinges in a boundary mirror called B. Due to the conservation of momentum at it, the tangential component of $\vec{k}$ must be conserved, meaning that the reflected wave will follow the direction of the normalized Poynting vector $\vec{S_r}$ with normalized wave number $\vec{k_r}$.
In advance for the next section, for isotropic materials, the isofrequency curve is a circle, and the reflection is represented in Fig. 3.9. The incident beam encounters a boundary where it is reflected satisfying the condition from Eq. (3.1). In this case, (the simplest case), the incident angle is the same as the reflection angle. The reflection is represented both in the isofrequency curve and with a COMSOL simulation (right of Fig. 3.9).
Looking at the COMSOL simulation, we can clearly see the incident wave, and distinguish between the Poynting vector and the wavevector. In the top right inset we schematically represent the process. We can see that, for this simple case, the wavevector and the energy goes in the same direction.

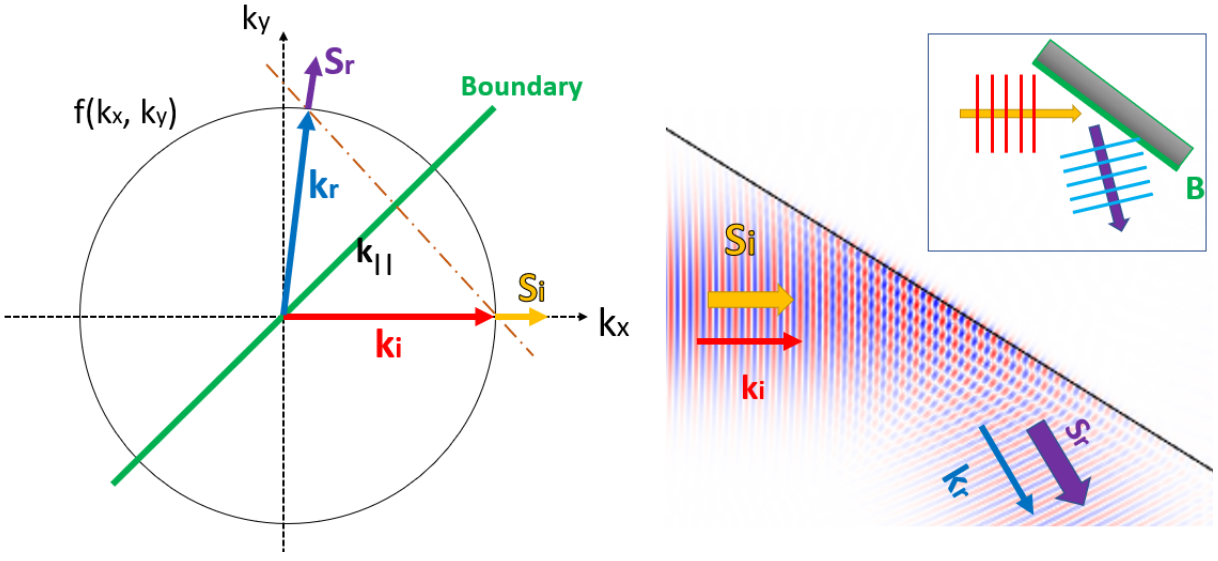

Figure 3.9: Isotropic material. On the left, it is represented the isofrequency curve, with the incident (red) and reflected waves (blue). There is a boundary mirror between them (green). On the right, it is represented the simulation in COMSOL, with the capability to distinguish between the Poynting vector and the wavevector. Top right inset schematically shows the result of the COMSOL simulation.

Note that for isotropic materials the Poynting vector and the wavevector are parallel, implying that the incidence angle θ_i and the reflected angle θ_r are equal, however, we will see that this can be very different in other media.

3.2.1 Isotropic material

As said above, we have already defined a Gaussian pulse (Chapter 2). Particularly, a Gaussian pulse is defined by a Gaussian function of the form:

$$f(x) = ae^{-\frac{(x-b)^2}{2c^2}} \tag{3.2}$$

In our COMSOL program, $b = 0$, $a = 1$, $x = y$ (we defined it in the y-direction) and $2c^2 = w0^2$. The parameters that we are going to change are the permittivity, the wavelength and the spot radius. Changing the permittivity is obvious because we have to try different media, but it also implies changing the absorption of the media, so, sometimes, it is necessary to change the wavelength too.
Previously, we have defined the permittivity by a diagonal tensor, but now we will use an isotropic tensor (in **Wave Equation, Beam Envelopes 2**). First, we work whit a medium with $\epsilon_r = 2.50$, so $n_{crystal} = 1.58$ and the results are shown in Figure 3.10.
In this case, the result follows the most common form of the Snell's law, as the incident ray makes 58° with the normal[2], the reflected beam occurs at the same 58°. What we see is specular reflection, because the second medium (air) has a lower refraction index. We can also see that, in this isotropic material, the Poynting vector and the wavevector are parallel.
Then, we can compare these results with another isotropic material, for example, let us try a isotropic medium with relative permittivity $\epsilon_r = 3.5$, one more unit than in the previous case, this simulation is represented in Figure 3.11. In this case $n_{crystal} = 1.87$, and the reflection angle is the same.
In both cases it is satisfied what we showed in Fig. 3.9, even when varying the permittivities, θ_i, θ_r are always equal and the Poynting vector, wavevector and group velocities are always parallel. However, the only difference is due to Beer's Law (Eq. (1.27)), the higher the permittivity the lower the intensity, because the absorption coefficient is directly proportional to the refraction index.
The only problem here is that we are not simulating SPs but rather light, because none of the permittivities is negative, however this problem can be extrapolated to SPs and a metal, but the simulation would have been more complicated because we would have had to previously excite the light.

[2]This can be calculated by trigonometry, knowing that we have a rectangle 64x90.

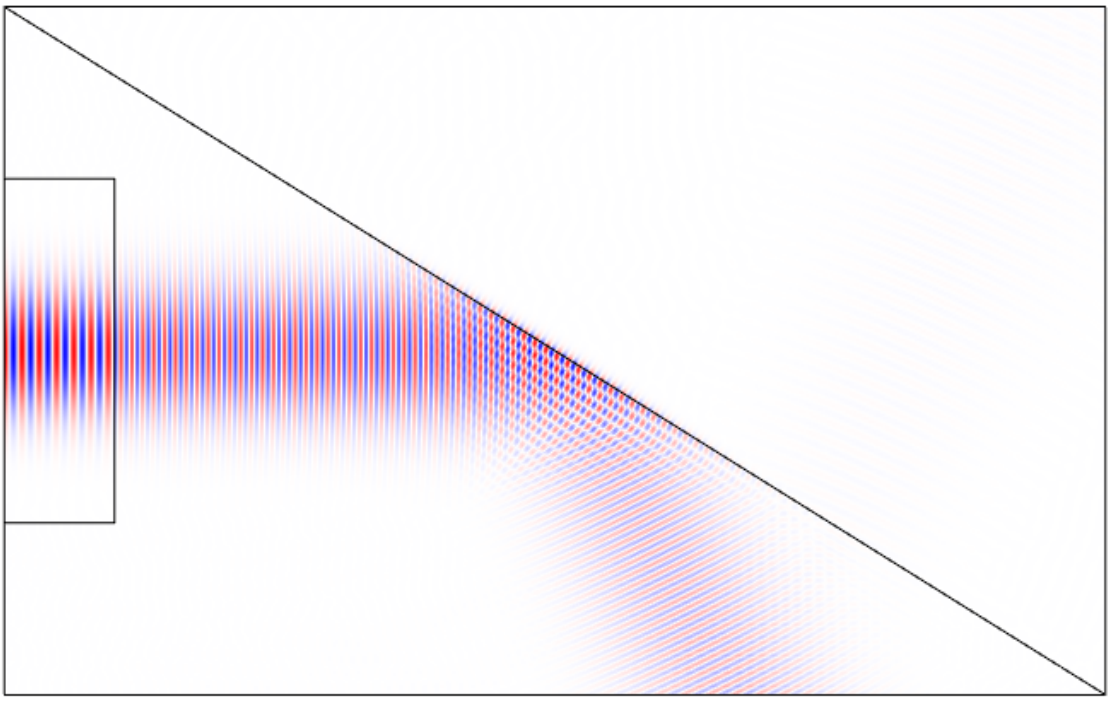

Figure 3.10: Simulation for an isotropic medium, with $\epsilon_r = 2.5$. It is a typical reflection, with angle 52°. The energy and the wavevector have the same direction.

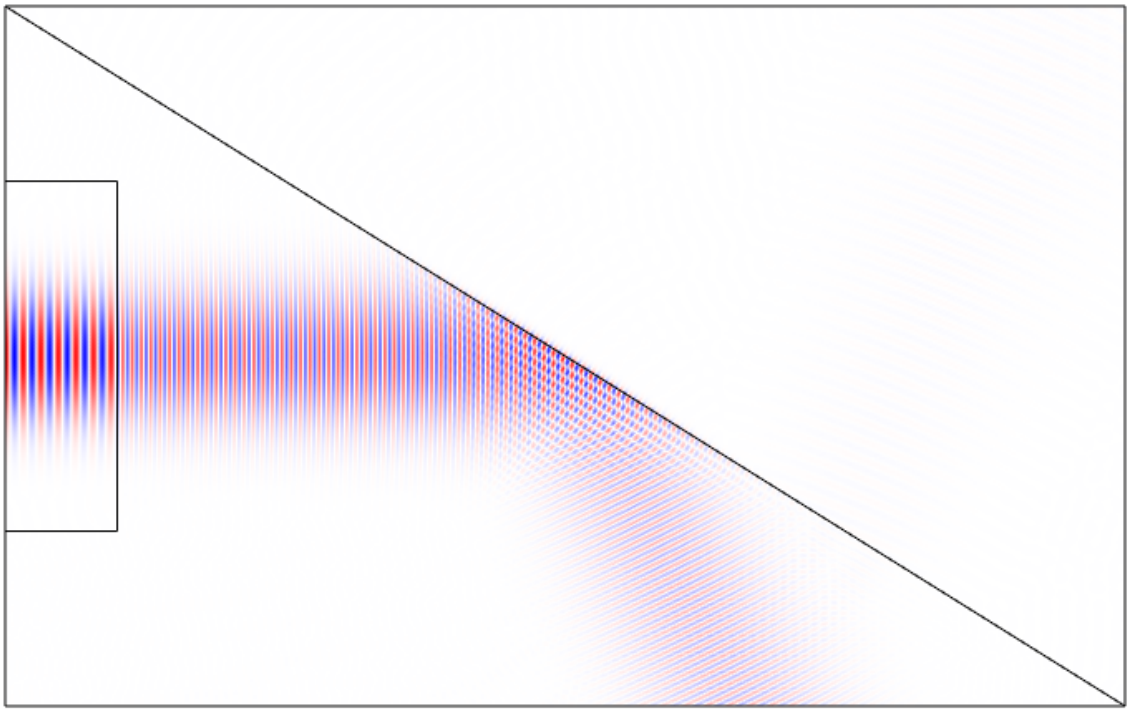

Figure 3.11: Simulation for an isotropic medium, with $\epsilon_r = 3.5$. The reflection is the same as in Figure 3.10.

3.2.2 Elliptic material

In an uniaxial material the isofrequency curve can be an ellipsoid, which implies 2 important related changes, first, depending on the incident wave, the Poynting vector might not be parallel to the wavevector, and so, the reflection angle is not the same than the incident angle.
For this case we cannot use an isotropic tensor, in **Wave Equation, Beam Envelopes 2**, we have to select a diagonal tensor in which one of the elements are different to the other two. We are going to try some different configurations and comment them.
First, we simulate a case where the optical axis is along the y-axis, with $\epsilon_y = 4$, whereas the other axis have $\epsilon_{x,z} = 3$, which means:

$$\epsilon_r = \begin{pmatrix} 3 & 0 & 0 \\ 0 & 4 & 0 \\ 0 & 0 & 3 \end{pmatrix} \tag{3.3}$$

Here, the reflection is represented in Fig. 3.12

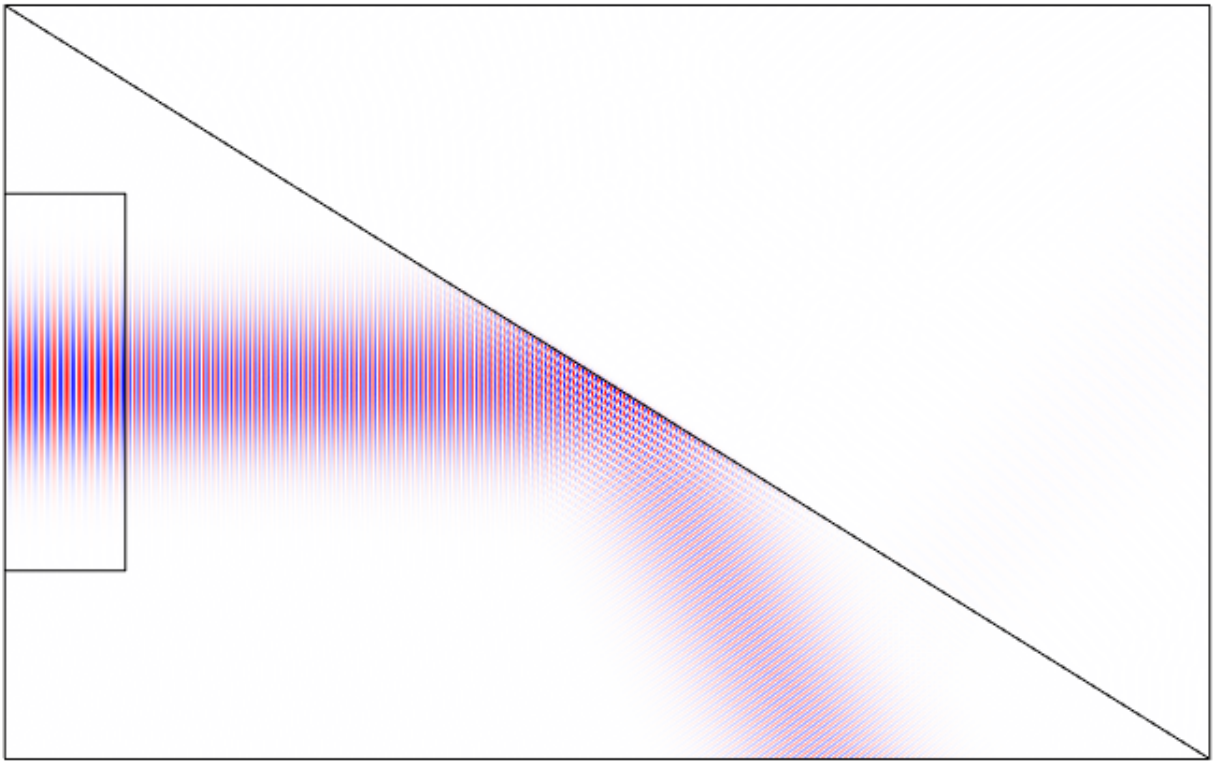

Figure 3.12: Simulation for an elliptic uniaxial medium. The incidence angle is different to the reflected angle, also the Poynting and $\vec{k}$ vectors have different directions.

Compared to the isotropic material, the reflection angle is a bit different, the main difference lies in the direction of the Poynting vector and the wavevector.
For the second try, we have to think about what would happen if, keeping the same optical axis we increase its norm.

$$\epsilon_r = \begin{pmatrix} 3 & 0 & 0 \\ 0 & 6 & 0 \\ 0 & 0 & 3 \end{pmatrix} \tag{3.4}$$

The result is represented in Fig. 3.13:

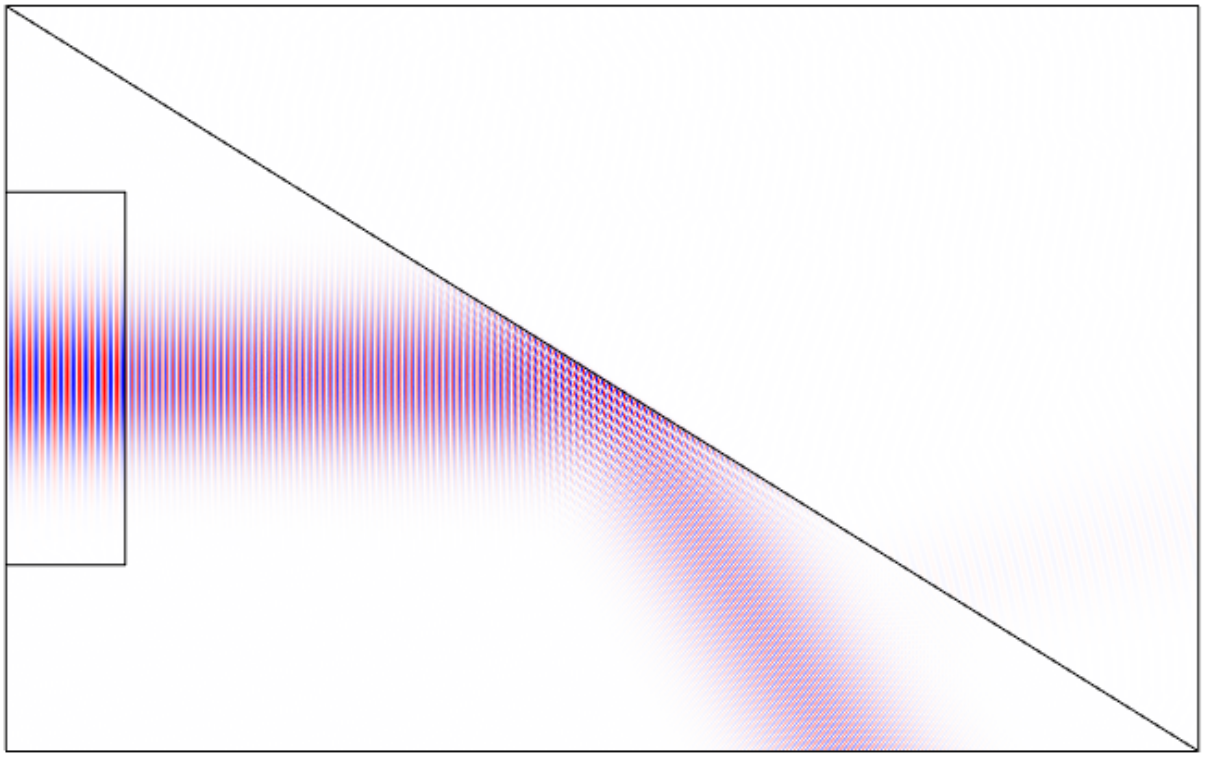

Figure 3.13: Simulation for an elliptic uniaxial medium. The reflected angle is different to that in the previous figure, and also the Poynting and $\vec{k}$ wavevectors have different directions.

We can better compare the reflection angles in Fig. 3.14, as we see, the difference is not very important, but the reflection changes in 5°. For the optical axis where $\epsilon_y = 4$, the angle is 66°, and for the optical axis with $\epsilon_y = 6$ the angle is 71°. There can be an error of about $\pm 1°$ in the calculation of the angles, but the difference is notorious and is still about 5°.
We are starting to distinguish a particular behaviour, changing the permittivity we can change the relationship between the incidence and reflection angles. Paying close attention to the wavevector and Poynting vector we can see another different behaviour, as said previously, they have different directions, but this difference is not as noticeable to other elliptical

cases.

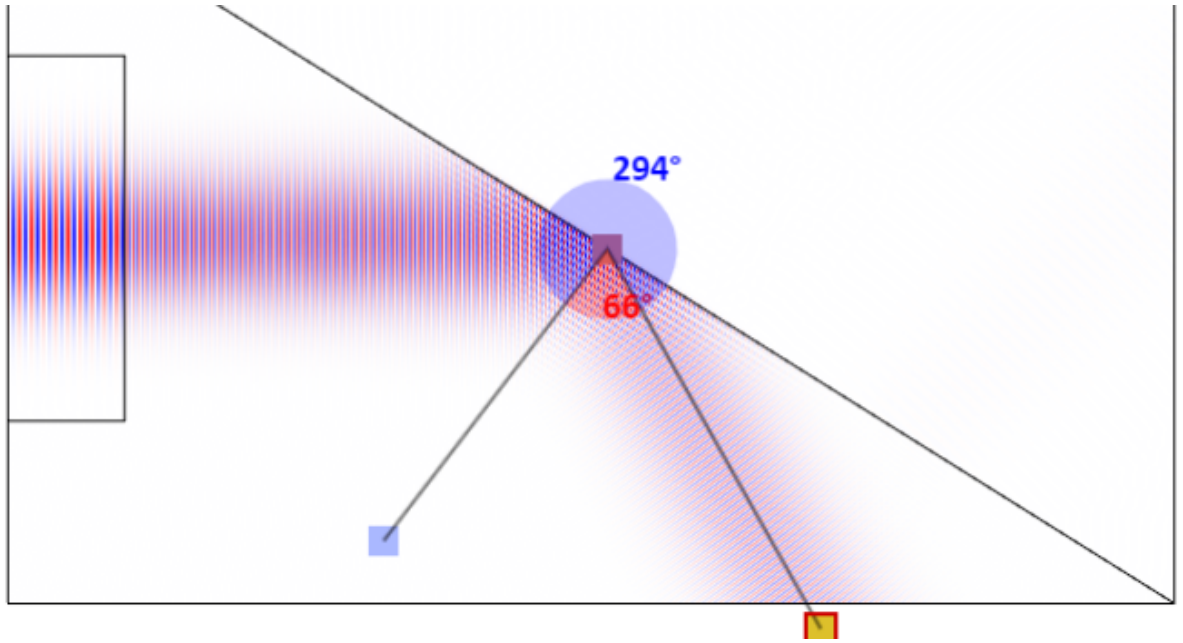

(a) Reflection angle of Fig. 3.12

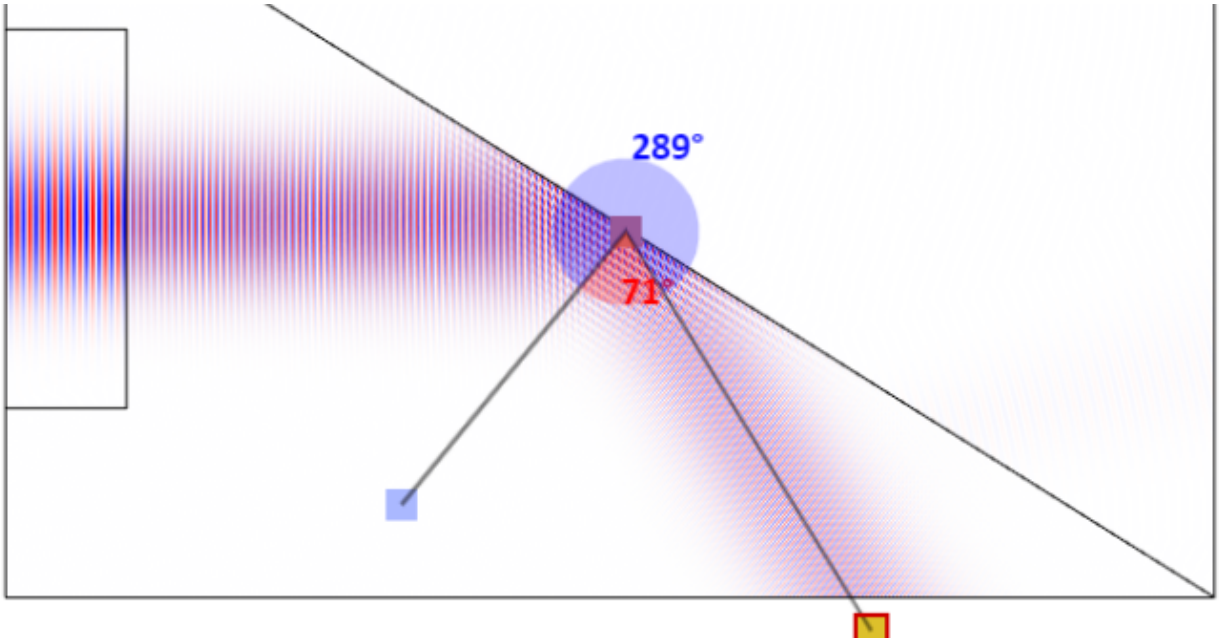

(b) Reflection angle of Fig. 3.13

Figure 3.14: Comparison between increasing the permittivity in the optical axis.

For the next simulation, let us change the optical axis to the z-axis:

$$\epsilon_r = \begin{pmatrix} 3 & 0 & 0 \\ 0 & 3 & 0 \\ 0 & 0 & 6 \end{pmatrix} \tag{3.5}$$

This results in:

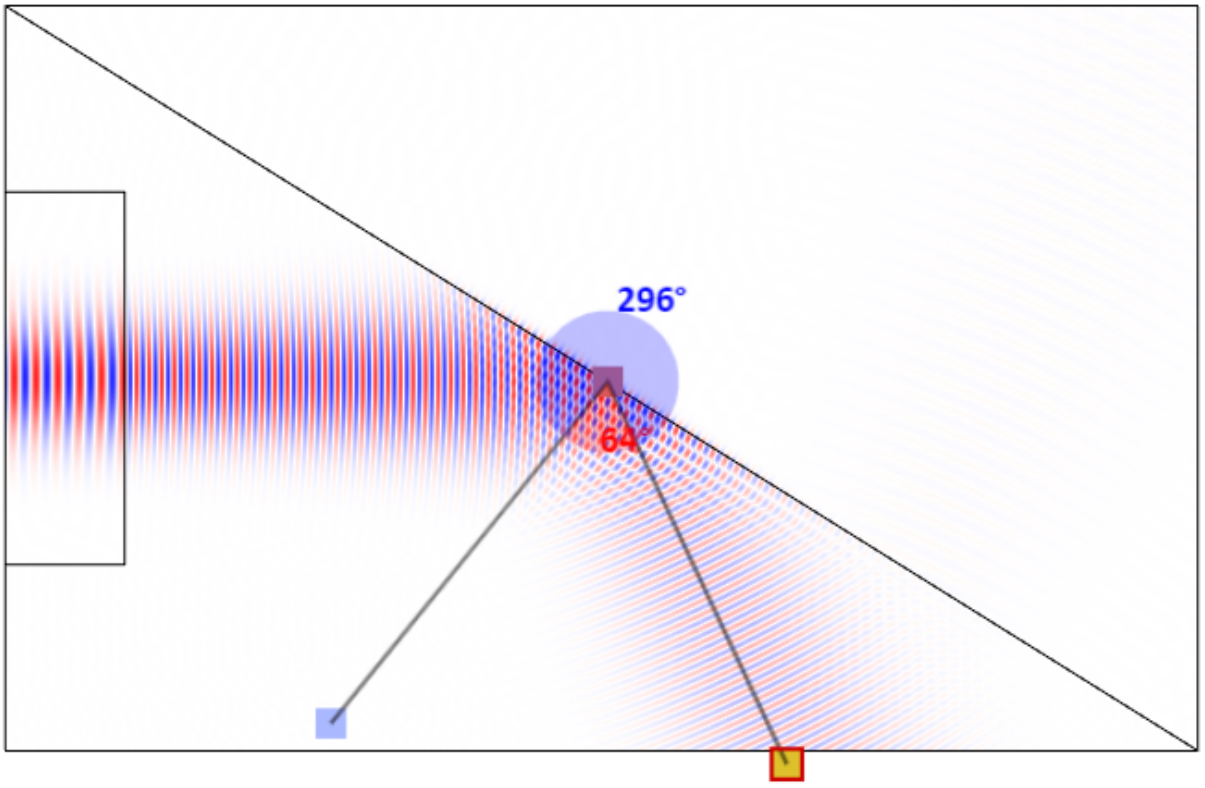

Figure 3.15: Simulation for an elliptical uniaxial medium, where the optical axis is the z-axis, and the permittivity tensor is represented in Eq. (3.5).

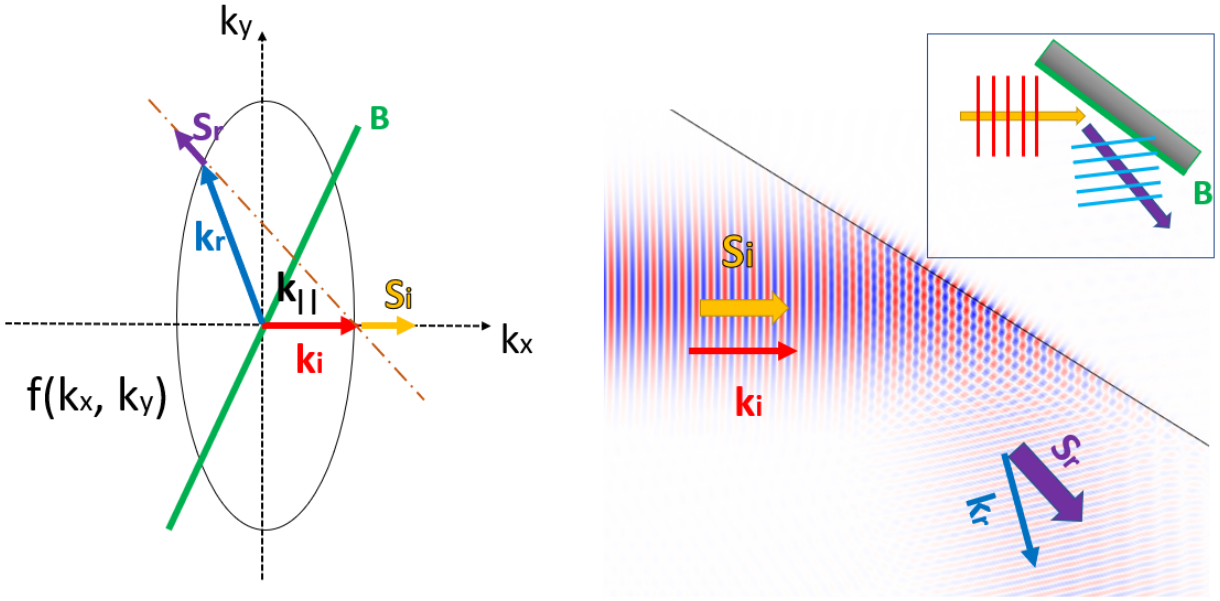

Figure 3.16: Elliptic uniaxial material. k_r and S_r are not parallel, and the reflected angle is different from the incident angle.

Setting the optical axis to the x-axis also results in a change in the reflection angle. As we see the reflection angle depends on the 3 values of the permittivity, and it is interesting to see how it changes and how is never the same than the incident angle, as it happens in an isotropic material.
This behaviour can be studied using the isofrequency curve, always satisfying the Eq. (3.1). For an elliptical material (Fig. 3.16) it does not follow the $\theta_i = \theta_r$ condition, so $\theta_i \neq \theta_r$, the condition that the system must follow is Eq. (3.1). As we see, for the reflected wave, k_r and S_r have different direction, meanwhile k_r follows the corresponding equation, S_r must be perpendicular to the isofrequency curve (in all points of the isofrequency curve).
On the left of Fig. 3.16, we see the isofrequency curve of an uniaxial material, similar to the previous case, instead of being a circle is an ellipsoid. Due to this ellipsoid shape, the reflection is different, we can see on the right of the picture how the wavevector goes and how the energy flows with different direction.

3.2.3 Hyperbolic material

A hyperbolic material can be either uniaxial or biaxial, and they can generate 2 types hyperbolic isofrequency curves, depending on the values of the permittivity. Type I hyperbolas occur when one of the permittivities is negative, and Type II, when 2 of the ϵ_i are negative. This fact generates very exotic materials with interesting properties and very uncommon refractions.
In hyperbolic materials, the medium has a behaviour as a metal along certain directions (those with a negative ϵ_r), however, the medium has a dielectric behaviour along the other directions.
Sometimes, the direction between the wavevector and the Poynting vector can be extreme, and they can be, for example, perpendicular at some points.
First, let us start with a Type I refraction with:

$$\epsilon_r = \begin{pmatrix} 2 & 0 & 0 \\ 0 & 1.8 & 0 \\ 0 & 0 & -1.5 \end{pmatrix} \tag{3.6}$$

In this case, the metallic optical behaviour corresponds to the z-axis, which is the axis that comes out of the plane, so it does not affect the result too much, look at Fig. 3.17.
The result is a refraction angle of 55°, about 10 degrees difference whit the previous cases, but the most interesting fact is that, due to the metallic behaviour in one direction there are SPs in the boundary.

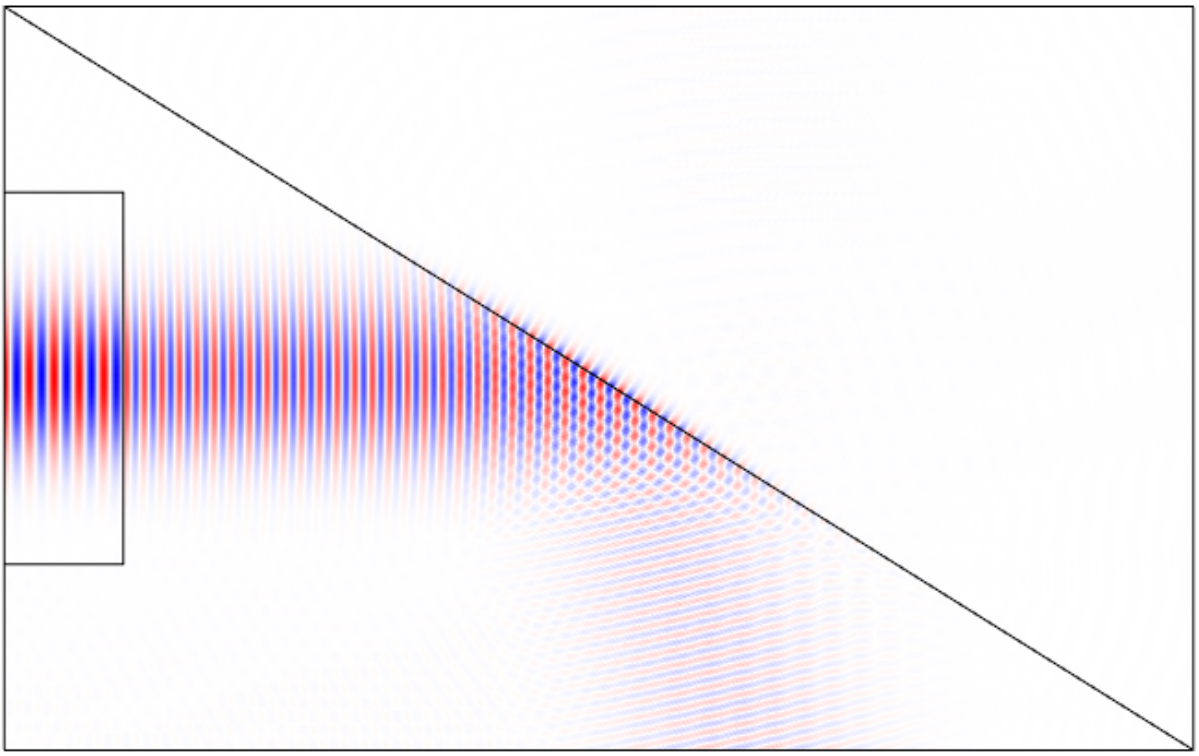

Figure 3.17: Simulation of a hyperbolic biaxial medium, represented in Eq. (3.6), as the negative permittivity is not in this plane the reflection is similar to previous results, but looking at the boundary we can see SPs.

The next step is to think what happens if we change the negative permittivity to the x-axis[3], we have tried the following configuration:

$$\epsilon_r = \begin{pmatrix} -1.3 & 0 & 0 \\ 0 & 2 & 0 \\ 0 & 0 & 2 \end{pmatrix} \tag{3.7}$$

The result is represented in the next figure.
This simulation is not fully optimized there are some background noise that I cannot improve, but fortunately it does not affect to the result, so we can use this simulation. The background noise is created because the negative value is in the x-axis which is in the same plane as the material, so the computer needs more power and accuracy, that is, reduce the grid size.

[3]We cannot set a negative permittivity in the y-axis because is the axis where the incident ray goes through, so if it is negative it behaves as a metal and the wave is only reflected and never enters in the crystal. However, exciting the wave in a certain way it is possible to set a negative value and obtain results.

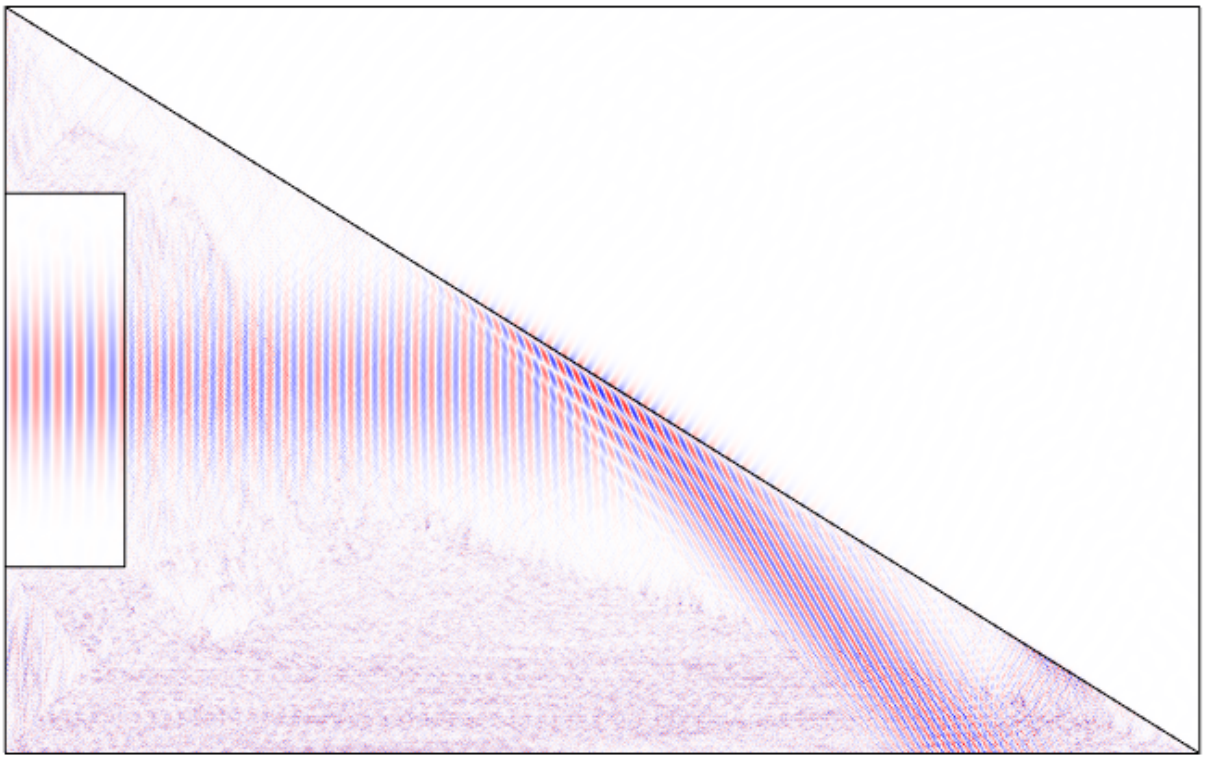

Figure 3.18: Simulation of a hyperbolic Type I reflection, where the negative ϵ corresponds to the x-axis. This simulation is not fully optimized, as we see there are a lot of noise background, but it does not affect to the result. We can see SPs at the boundary. The Poynting vector and wavevector have very different directions and the refraction angle is 77°.

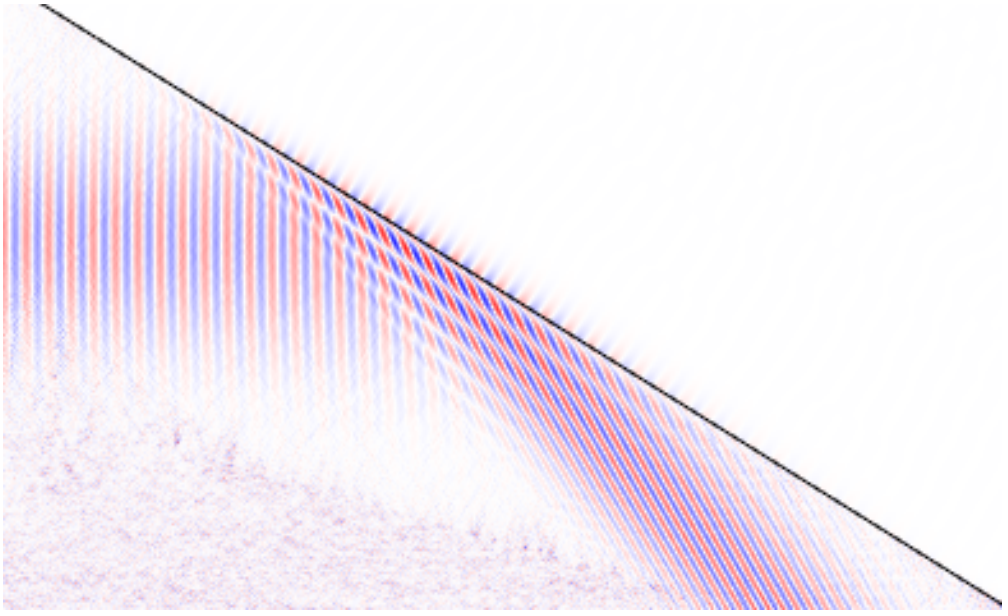

Figure 3.19: Zoom into the boundary, we can see perfectly the SPs and the difference between Poynting vector and wavevector directions.

In this case the refraction angle is 77°, a strong difference between other cases, remember that the incidence angle is 58°. However, we have already seen the difference between incident and reflection angles in previous cases, here, another important difference is given in the relationship between the Poynting vector and the wavevector. In this simulation, there is the most notorious non-collinearity between them, we can see it better if we zoom it, represented in Figure 3.19, the two vectors are near to be perpendicular.
There are also SPs due to the metallic behaviour, this did not happen in the previous cases. This reflection is explained by the isofrequency curve in this way:

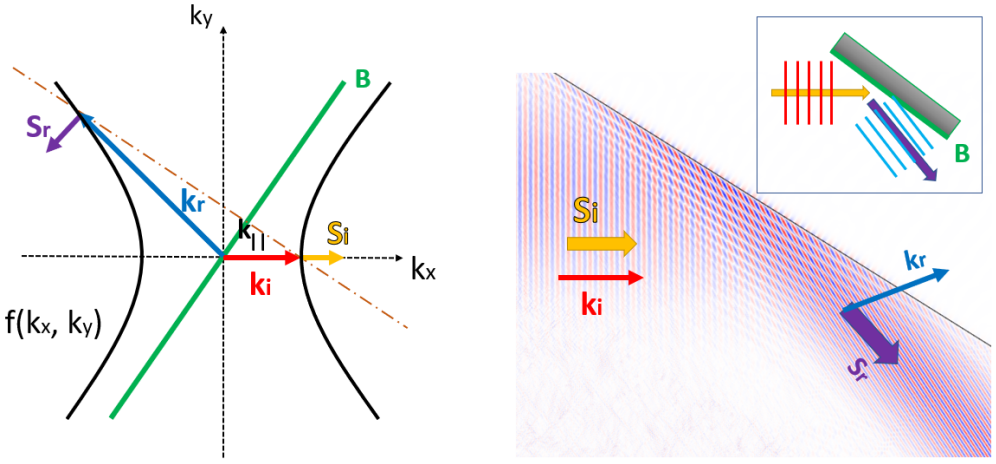

Figure 3.20: Biaxial material. In this case we see an hyperbolic reflection, in which the reflected angle is more extreme than in previous cases, and k_r and S_r are very close to be perpendicular.

Here, we have to highlight 2 facts, in the one hand, the material has a strong anisotropy, having different optical properties in each directions, and on the other hand, the incident and reflected waves must satisfy momentum conservation, these two facts lead to exotic reflections.
Then, we have tried Type II hyperbolic refraction, having this type of material the reflection could be more exotic, we have started with this tensor:

$$\epsilon_r = \begin{pmatrix} -1.3 & 0 & 0 \\ 0 & 2 & 0 \\ 0 & 0 & -2 \end{pmatrix} \tag{3.8}$$

We have only change the sign of ϵ_z, the numerical values are the same, and the result is the same as for Eq. (3.7), so we can conclude:
First, we can se the emergence of SPs with one negative permittivity, because it adds a metallic optical behaviour, however, having 2 negative permittivities does not improve the SPs with respect a only one negative value, and also, having 2 negative ϵ_i creates more

background noise, so we will only use one negative permittivity in the z-axis.
Second, having the negative permittivity in the plane where the ray goes through (x-axis in this case) has a strong relation with the changing in the directions of $\vec{S}$ and $\vec{k}$, because it affects stronger to the isofrequency curve with our incidence angle.
Now, our goal could be to find an exceptional reflection. Exploring with these materials we have found a interesting behaviour, keeping constant ϵ_y and decreasing the absolute values of ϵ_x and ϵ_y the reflection angle becomes bigger with respect to the normal, on the other hand, increasing these values (ϵ_x and ϵ_y), the reflection angle gets closer and closer to the normal, and, on a certain moment, the reflection angle becomes negative.
When the reflection angle is negative this reflection is known as a negative or anomalous reflection. Trying different configurations, we have found the following:

$$\epsilon_r = \begin{pmatrix} 12 & 0 & 0 \\ 0 & 1.65 & 0 \\ 0 & 0 & -12 \end{pmatrix} \tag{3.9}$$

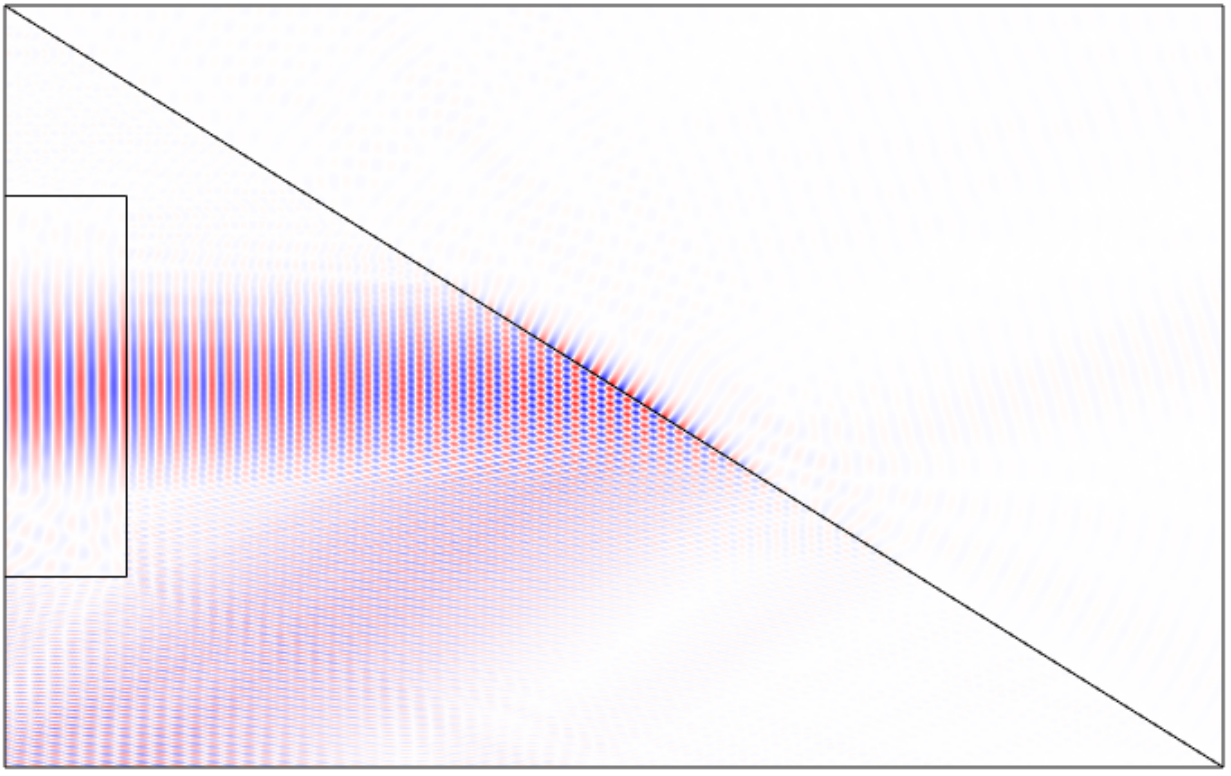

Figure 3.21: Anomalous reflection in a hyperbolic material. The reflection angle is negative, -21°.

In this very exotic case of anomalous reflection (Fig. 3.21), the reflection angle is $-21°$ with respect the normal, and we still see very intense SPs on the surface of the boundary. This

reflection is very exotic and important, this strongly anisotropic SPs come from the strong anisotropy of the crystal (the medium in which they propagate).
But, there is also a more strange case, a very particular case called backreflection, in which $\theta_i = -\theta_r$ and the incident and reflected waves are overlapped. This case is common, for example, in a mirror, in which this occur for a normal incidence, but seeing this behaviour with an incidence angle of 58° is very exceptional.
This case can occur due to different reasons: a different incidence angle, different angles of the interface between the hyperbolic material and the dielectric, or, (as we do) with specific values of the permittivity. This reflection can be shown in the isofrequency curve as follows:

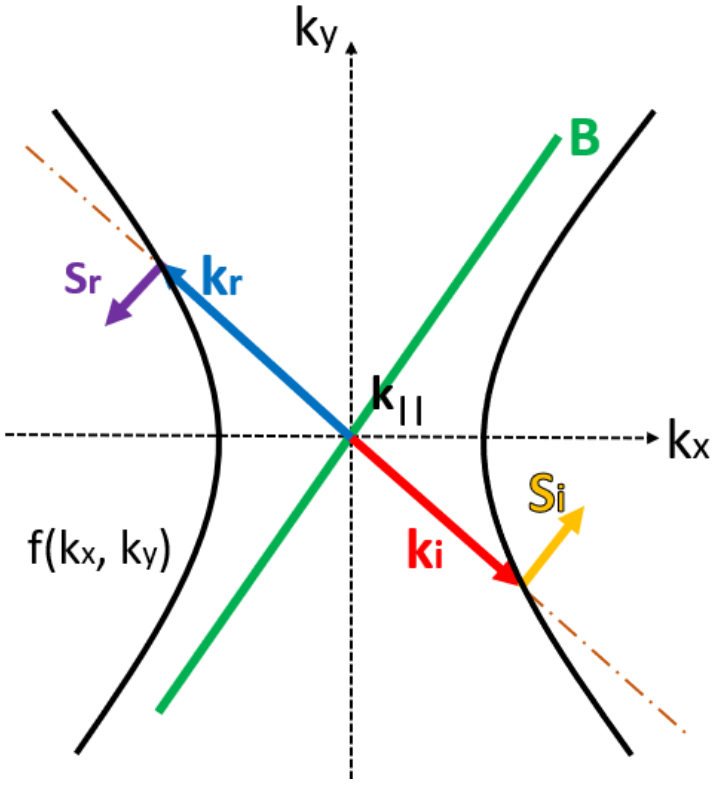

Figure 3.22: Isofrequency curve for a hyperbolic backreflection. A very particular case for hyperbolic materials.

Here (Fig. 3.22), due to the shape of the isofrequency curve, the result is even more anti-intuitive. Vectors k_r and S_r are perpendicular, and S_r is opposite to S_i. The direction in which the wave flows is given by the energy (the Poynting vector), being S_r opposite to S_i means that the reflected wave comes back.
This is a extreme case for the hyperbolic reflection, as we have said, called backreflection, because the wave goes back to the source in non-intuitive angles.

We have simulated a back-reflection with the following configuration:

$$\epsilon_r = \begin{pmatrix} 15 & 0 & 0 \\ 0 & 5.75 & 0 \\ 0 & 0 & -15 \end{pmatrix} \tag{3.10}$$

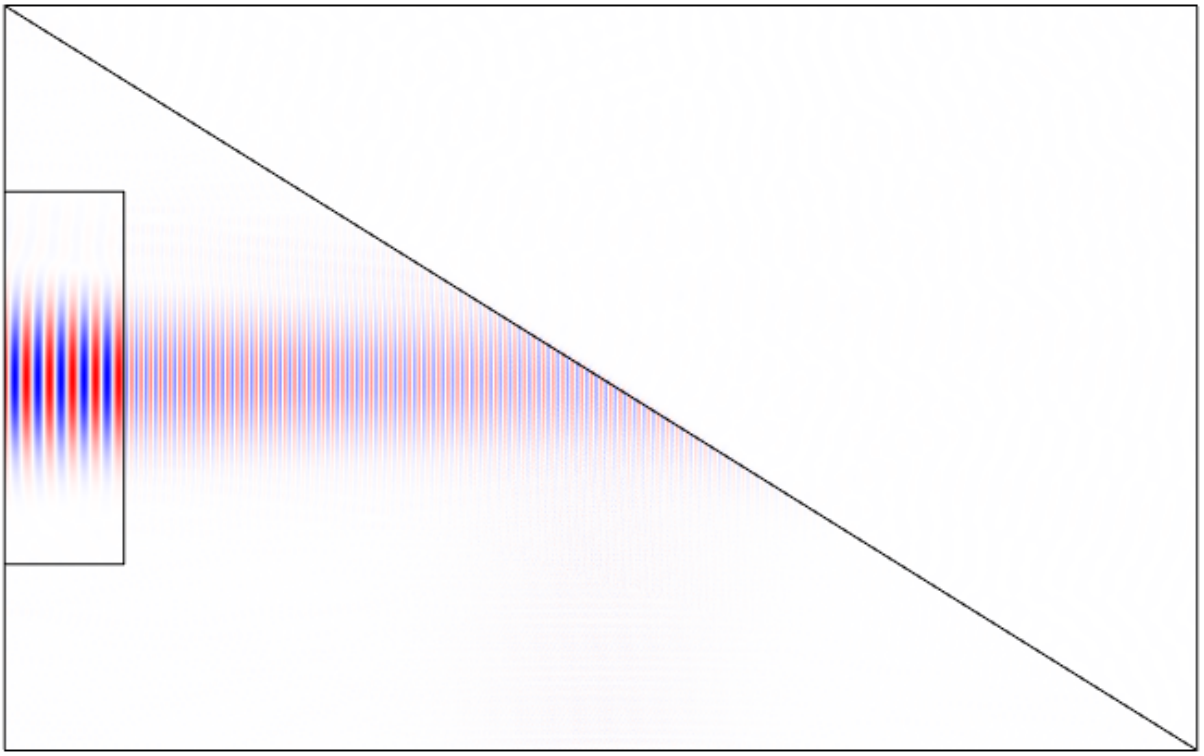

Figure 3.23: Hyperbolic backreflection. The reflected wave is overlapped to the incident wave. Ver exotic case.

This back-reflection can be very elusive and difficult to measure, what is more, in the research group this has not yet been measured, however, we have demonstrated that this phenomenon is possible, so our final point will be a experimental proposal to measure it in a laboratory.

3.2.4 Experimental proposal

Taking into account that this thesis is theoretical, we are not going to describe the experimental setup with many details, however, it is interesting to show that this is possible and can happen in real life and using SPs instead of light, as in the simulations.
The $\alpha - MoO_3$ is a natural Van der Walls material, which at certain frequencies is hyperbolic, and thus it is possible to visualize and verify SPs in $\alpha - MoO_3$ flakes and disks using nano-

imaging and nano-spectroscopy. These imaging techniques can be realized with a s-SNOM, a scattering-type scanning near-field optical microscope [16].
The s-SNOM has a tip to which we focus a laser beam. This way the tip is able to excite SPs into the material, and we can only detect with the tip the back-reflected ones, which means that it can be used to measure back-reflections.
Once the flake is created, it is possible to create on it an air boundary (like the one in the simulation) using a focused ion beam technique. Having the two media, crystal-air, and then, experimentally, using the tip of the as antenna, take a near-field s-SNOM image of the polaritons that are back-reflecting on the air boundary previously created.
As we have said, how we send and detect the polaritons from the tip, only the back-reflected waves are detected, so this experimental propose can be a good choice to reproduce the last point.

Chapter 4

Conclusions

In this master thesis we have introduced the basics about nanooptics, focused in surface polaritons, but simulated in this work with light to simplify the computational problem, being aware that all the results obtained can be directly extrapolated to SPs. We have shown that reflections are not always as simple as the most common form of the Snell's law predicts, introducing different media such as isotropic, uniaxial, biaxial an hyperbolic materials.
Using the program COMSOL we have simulated these different materials. First of all, with the first simulations, we obtain a conclusion for simulations in this field:

- It is very important to achieve an equilibrium between computational cost and results, especially when calculations become more and more harder. We have shown the importance of the mesh, and how having a finer mesh result in better results, but obviously requires more computational cost.

The mesh size has a more significant influence when one of the permittivities are negative (thus supporting SPs), so a finer mesh is required.
Focusing on the reflection results, we have simulated three different types of materials:

- Isotropic: the material has only one permittivity value (one refractive index), so the result satisfies the most common form of the Snell's law, being $\theta_i = \theta_r$.

- Uniaxial/biaxial: the crystal has an optical axis along with the permittivity is different to the other directions of space. The Snell's law is not satisfied in its common form, and the reflection needs to be derived from the isofrequency curve taking into account momentum conservation. The main result was that $\theta_i \neq \theta_r$, and that, with negative permittivities SPs emerge on the boundary.

- Hyperbolic: this type of material yields the most exotic results. Generally, two values of the permittivity are negative, so the crystal acquires a metallic optical behaviour

in these directions. One of the most interesting result was the anomalous reflection in which the reflected angle is negative. Also, the other interesting result was the condition for back-reflection, in which $\theta_i = -\theta_r$, overlapping the incident wave with the reflected one at angles very different to that for normal incidence.

The back-reflection process has not been experimentally measured in hyperbolic media, however, in this thesis we have proposed an experimental way to reproduce and study this phenomenon.

The whole scope of the exotic materials that we have used with the emergence of SPs with novel characteristics demonstrate that nanooptics are a very interesting field. So far, we have simulate some aspects of reflection in these media, the next step would be translating them to the lab.

I

References

Bibliography

[1] Gonzalo Álvarez Pérez (2018): "Polaritons in biaxial crystals", Master thesis.

[2] Barnes, W., Dereux, A. and Ebbesen, T. (2003): "Surface plasmon subwavelength optics". *Nature*, **424**, 824-830. https://doi.org/10.1038/nature01937

[3] Chen, J., Badioli, M., Alonso-González, P., Thongrattanasiri, S., Huth, F., Osmond, J., Spasenović, M., Centeno, A., Pesquera, A., Godignon, P., Zurutuza Elorza, A., Camara, N., Javier García de Abajo, F., Hillenbrand, R. and Koppens, F. H. L. (2012): "Optical nano-imaging of gate-tunable graphene plasmons". *Nature* **487**, 77–81.

[4] Li, P., Lewin, M. Kretinin, A. V., Caldwell, J. D., Novoselov, K. S., Taniguchi, T., Taubner, T. (2015): "Hyperbolic phonon-polaritons in boron nitride for near-field optical imaging and focusing". *Nature Communications* **6**, 7507.

[5] Nikitin, A., Yoxall, E., Schnell, M. Vélez, S., Dolado, I., Alonso-Gonzalez, P., Casanova, F., Hueso, L., Hillenbrand, R. (2016): "Nanofocusing of Hyperbolic PhononPolaritons in a Tapered Boron Nitride Slab". ACS Photonics, **3** (6), pp 924–929.

[6] Ma, W., Alonso-González, P., Li, S., Nikitin, A. Y., Yuan, J., Martín-Sánchez, J., Taboada-Gutiérrez, J., Amenabar, I., Li, P., Vélez, S., Tollan, C., Dai, Z., Zhang, Y., Sriram, S., Kalantar-zadeh, K., Lee, S. T; Hillenbrand, R., Bao, Q. (2018): "InPlane Anisotropic and Ultra-Low Loss Polaritons in a Natural van der Waals Crystal". *Nature* **562**, 557–562 (2018). https://doi.org/10.1038/s41586-018-0618-9.

[7] Maxwell, J. C. (1873): *A Treatise on Electricity and Magnetism*, Vol. 2, Oxford.

[8] Bertolotti, M., Sibila, C., and Guzmán, A. M. (2017): *Evanescent Waves in Optics: An Introduction to Plasmonics*, Vol. 206, Springer, 251p.

[9] Landau, L. D. and Lifshitz, E. M. (1960): *Electrodynamics of Continuous Media*, Vol. 8 of the Course of Theoretical Physics (Pergamon Press), §78 and §79.

[10] Gary P. Misson (2010): "The theory and implications of the biaxial model of corneal birefringence". Ophthalmic and Physiological Optics **30**(6): 834-46. DOI:10.1111/j.1475-1313.2010.00782.x.

[11] Shekhar, P., Atkinson, J. and Zubin, J. (2014): "Hyperbolic metamaterials: fundamentals and applications". *Nano Convergence* **1**, 1.

[12] Basov, D. N., Fogler, M. M., García de Abajo, F. J. (2016): "Polaritons in Van der Waals materials." *Science* **354**, 6309.

[13] Joshua D. Caldwell, Lucas Lindsay, Vincenzo Giannini, Igor Vurgaftman, Thomas L. Reinecke, Stefan A. Maier and Orest J. Glembocki (2015): "Low-loss, infrared and terahertz nanophotonics using surface phonon polaritons". *Nanophotonics* **4**(1):44-68. 10.1515/nanoph-2014-0003.

[14] https://www.comsol.com/products

[15] Alejandro Muñoz Manterola (2018): "Control of nanolight in 2D Materials". End-of-Degree Thesis.

[16] Weiliang Ma, Pablo Alonso-González, Shaojuan Li, Alexey Y. Nikitin, Jian Yuan, Javier Martín-Sánchez, Javier taboada-Gutiérrez, Iban Amenabar, Peining Li, Saül Vélez, Christopher Tollan, Zhigao Dai, Yupeng Zhang, Sharath Sriram, Kourosh Kalantar-Zadeh, Shuit-tong Lee, rainer Hillenbrand and Qiaoliang Bao (2018): "In-plane anisotropic and ultra-low-loss polaritons in a natural van der Waals crystal". *Springer Nature Limited* **562**, 557–562. https://doi.org/10.1038/s41586-018-0618-9.